



University of Fribourg (Switzerland)

Department of Physics

**Natural and Artificial Radioactivity
Monitoring at the High Altitude Research
Station Jungfraujoeh: Installation and Test
of a New High Volume Aerosol Sampler in
combination with Laboratory
Gamma-Spectroscopy**

Master Thesis in Experimental Physics

by

Thomas Flury

from Kleinlützel/SO (Switzerland)

Under the supervision of Prof. Dr. Hansruedi Völkle

Fribourg, October 2006

Contents

1	Introduction	1
1.1	History of air radioactivity monitoring in Switzerland	2
2	Radioactivity	4
2.1	Laws	4
2.2	Radioactive equilibrium	5
2.3	Decay modes [1]	7
2.3.1	Alpha decay	7
2.3.2	Beta decay	7
2.3.3	Electron capture EC	8
2.3.4	Gamma transition	9
2.4	Natural Radioactivity	9
2.4.1	Natural Radioactivity in Air	15
2.4.2	Measurement	15
2.4.3	Calculations	15
3	Atmosphere	19
3.1	Troposphere	19
3.2	Stratosphere	19
3.3	Mesosphere	20
3.4	Thermosphere	20
3.5	Aerosols	21
4	Cosmic rays	23
4.1	Production of beryllium 7 and beryllium 10 radio nuclides	24
4.1.1	Stratosphere to Troposphere Exchange [4]	24
4.1.2	Seasonal variations in surface-air beryllium concentrations	26
4.2	Radioactivity in air	27
5	Gamma Spectrometry [2]	29
5.1	Interaction of gamma rays with material	29
5.1.1	Photoelectric effect	30
5.1.2	Compton scattering	31
5.1.3	Pair production	31
5.2	Interaction with the detector	32
5.2.1	The large detector	33

5.2.2	The small detector	33
5.2.3	The real detector	33
5.3	High purity germanium crystals	33
5.4	Calibration of the Multi Channel Analyzer MCA	35
5.4.1	Energy calibration	35
5.4.2	Peakform calibration	36
5.4.3	Efficiency calibration	36
5.4.4	Absorption in the sample	37
5.4.5	True coincidence summing	37
5.4.6	Suitable nuclide mixtures	37
5.4.7	Execution of the calibration	39
5.5	Peak calculations	39
5.5.1	Peak search	40
5.6	Software	41
5.6.1	InterWinner TM analyzing program	41
5.6.2	Decay correction	42
5.6.3	Decay correction during sampling time	43
5.7	GESPECOR	43
5.8	Uncertainty budget	46
6	Digitel DHA-80	48
6.1	Air Volume	49
7	Measurements	53
7.1	Goals	53
7.2	Procedure	53
7.3	Sampling in Fribourg	55
7.3.1	Results	55
7.4	Sampling at Jungfrauoch	56
7.4.1	Results	60
7.5	Comparison Jungfrauoch-Fribourg	61
7.5.1	Comparison of the Swiss results to those of PTB and DWD	63
7.6	Air radioactivity sampling with aircraft of the Swiss army in the lower stratosphere	63
7.7	Correlation to precipitation	65
7.7.1	Oberschrot	65
7.7.2	Fribourg	65
7.7.3	Fine dust concentrations	65
7.8	Test of filtering material	69
7.9	Anticorrelation of Beryllium and solar activity	72
8	Conclusions	74
8.1	Digitel combined with ORTEC Detective	74
8.1.1	Advantages of Digitel	75

8.2	Detection Limits	76
8.3	The GAW Program of the WMO	76
8.3.1	The Central European Baseline Station	77
8.3.2	Contribution of the Radioactivity Section (SUER)	78

List of Figures

1.1	Global nuclear weapon tests	3
2.1	Thorium Series	10
2.2	Uranium Series	12
2.3	Actinium series	12
3.1	The atmosphere	20
3.2	Sedimentation velocity of aerosols	22
4.1	Cosmic Ray Energy	25
4.2	Cross sections for ^7Be production	25
4.3	Radioactivity in air	28
5.1	Gamma Spectrometer set up	30
5.2	Attenuation coefficient for Compton, pair prod. and photo effect	32
5.3	The large and small Detector	34
5.4	The real Detector	34
5.5	Different types of spectra	34
5.6	True Coincidence Summing	38
5.7	Peak calculation	40
5.8	Peak search	41
5.9	GESPECOR Detector file	44
5.10	GESPECOR Geometry file	45
5.11	GESPECOR self attenuation correction	45
6.1	Digitel DHA-80 in Fribourg	49
6.2	Scheme of Digitel	50
6.3	Digitel controlled via Internet	50
7.1	Detector OX	54
7.2	Spectrum	57
7.3	All Fribourg data	58
7.4	Rain in Fribourg	58
7.5	Comparison Fribourg-Jungfrauoch	62
7.6	PTB, DWD and Fribourg	62
7.7	Oberschrot 2004	66
7.8	Oberschrot 2005	66

7.9	Oberschrot more in detail	67
7.10	Filter with Saharan dust	69
7.11	Beryllium 1991-2006	73
7.12	Solar cycle	73
8.1	Digitel and Ortec Detective	75
8.2	GAW stations	78
8.3	GAW	78

List of Tables

2.1	Thorium series $A=4n$	10
2.2	Uranium series $A=4n+2$	11
2.3	Actinium series $A=4n+3$	13
2.4	Natural radioactivity	14
5.1	Nuclide mixture for energy calibration	35
5.2	Nuclide mixture	38
5.3	GESPECOR correction factors	46
7.1	Fribourg data	59
7.2	Jungfrauoch	60
7.3	Comparison Jungfrauoch	61
7.4	$^{10}\text{Be}/^7\text{Be}$	63
7.5	High altitude filters	64
7.6	Fine dust Fribourg	68
7.7	Filter test	71
7.8	Two layer filter test	72
8.1	Detection Limits	77

1 Introduction

This Master Thesis contains the following parts: The first part aims to introduce gamma spectrometry and the new high volume air sampling system Digitel DHA-80. The second part analyses installation and testing at the High Altitude Research Station Jungfrauoch and compares the results to other measurements.

The Digitel DHA-80 High Volume Air Sampler (HVS-2) is a new instrument run by the Swiss Federal Office of Public Health (SFOPH) in order to improve their network of measuring ambient radioactivity. It has an air flow rate of 6 to 60 m³/h and aerosol particles are collected on round glass fibre filters. The Section for environmental radioactivity (SUER) runs several instruments widely distributed in Switzerland to measure the radionuclide concentration in ambient air. There are two different systems: RADAIR and the first generation high volume samplers HVS-1. RADAIR measures automatically gross α - and β -activity at 11 stations, providing online data every half an hour, whereas the HVS-1 system collects aerosols at 5 different stations and measures γ -ray emitters once a week in the laboratory by germanium gamma spectrometry. The HVS-1 system is much more sensitive (detection limit of 0.1 μ Bq/m³ vs. 0.5 Bq/m³) than the RADAIR system, but one has to wait one week for the results.

The goal of the new instrument is to improve the existing HVS-1 stations by providing on-line radioisotope data in the future. Up to now the sampled filters have to be sent to the laboratory where a gamma-ray spectrum is obtained in 1-2 days. The idea is to equip the Digitel High Volume Air Sampler directly with a germanium detector and to measure the filters right after filter change. The results could then be transmitted and obtained through Internet. Compared to the HVS-1 system data would then be obtained faster with the new system, although it would remain slower but much more sensitive than RADAIR.

Two Digitel instruments were first tested at Fribourg. One of them was positioned during this work on the High Altitude Research Station Jungfrauoch at 3454 m asl. The other one is currently in Fribourg but will be positioned at Rochers-de-Naye at 2042 m asl in the near future. The Digitel is very well suited for Jungfrauoch because there would not be sufficient space to run a HVS-1 instrument of the first generation, which has a flow rate of up to 600 m³/h. Moreover at Jungfrauoch it would be a technical challenge to heat such a high amount of air before its passage through the filter. The new one is small and compact and fits into the small space available at the Jungfrauoch.

There were many delays at the beginning of my work because of several software problems of the Digitel. They first had to be solved together with Digitel Elektronik AG before

we could move the instrument to Jungfraujoch. In attention of the final software update we decided to run both air samplers one next to the other and test different filtering materials all in use for aerosol monitoring on different air samplers. These tests took 3 months. After some technical installations the instrument could finally be moved to Jungfraujoch in May 2006.

As soon as the Digitel was installed at Jungfraujoch we started measurements every two weeks studying mixing and transport processes of aerosol bound radioactive isotopes in the atmosphere. The main elements of interest were the natural radionuclides ^7Be and ^{210}Pb . Due to their different origin- ^7Be is a cosmogenic and ^{210}Pb a terrestrial radionuclide- they can be used as tracers for atmospheric air mass transport. The results are compared to stations in Germany and to previous results from Fribourg. Evaluation of ^7Be data collected during the last 16 years show clear seasonal variations with maximum values in summer and minimum in winter. Moreover the anticorrelation of the cosmogenic ^7Be -activity concentration with the solar activity is evident. As a secondary activity, resulting from the public discussions about exceeded finedust concentrations, the filters were weighed to receive results about massconcentrations of finedust particles in air. These values are compared with values at Jungfraujoch which were provided by the EMPA.

The goal of the measurements at Jungfraujoch is to provide data about radionuclides for the GAW (Global Atmosphere Watch) Program. Jungfraujoch is worldwide one of 20 stations participating in this network and our data shall flow into it in the near future.

1.1 History of air radioactivity monitoring in Switzerland

Environmental monitoring of radioactivity started in Switzerland in 1956 with the appointment by the Swiss Federal Council of the Federal Commission for Radioactivity Surveillance. The reason was the concern about the constant rise in environmental radioactivity in the Northern Hemisphere as a consequence of the nuclear weapon tests in the 1950s and 1960s see figure 1.1. This led to international agreements, first to abandon atmospheric tests (1963: PTBT=Partial Test Ban Treaty), then to limit the power of tests to 150 kT (1974: Threshold Test Bann Treaty) and finally to a "Comprehensive Test Ban Treaty" (1996: CTBT).

As a consequence, Switzerland, similar to other countries, installed a network to monitor the radioactivity of air, rain, water, soil, grass, milk and other food, completed by measurements of the radionuclide content in the human body. Paul Huber, later his brother Otto Huber and then Heinz Hugo Loosli presided over this commission, which in 1957 addressed its first report to the Federal Council. In the following years, the monitoring program was constantly improved and adapted. The program first focused on the measurement of the atomic bomb fallout. Later, nuclear reactors, research institutions, industries and hospitals using radionuclides became of more interest. Today, automatic networks are operated for dose rate measurements and aerosol radioactivity

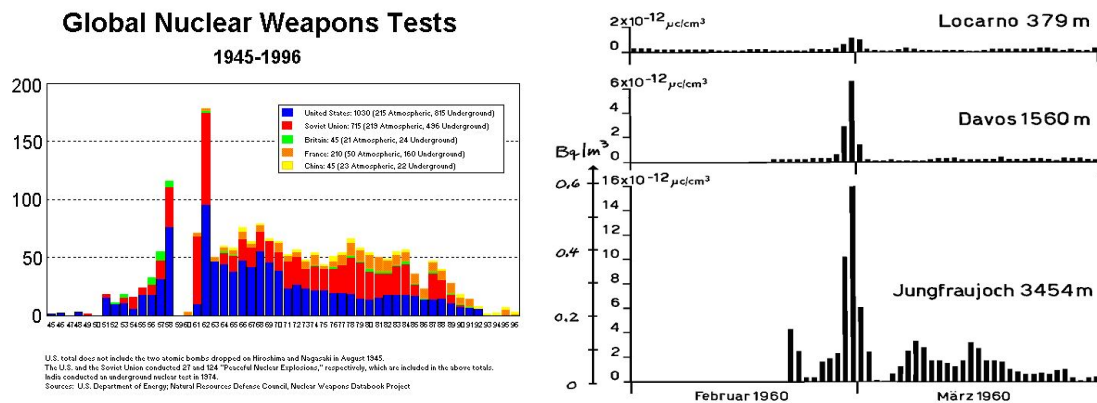


Figure 1.1: Amount of nuclear weapon tests since 1945 on the left (Source: Internet) and detection of the fallout of the first French atomic bomb test in the Sahara at Locarno, Davos and Jungfrauoch (Source: KUER-Bericht 1960).

(RADAIR), completed by high volume air samplers (HVS-1) and in situ Gamma Spectrometry. Since 1986, the Federal Office of Public Health has been responsible for the environmental monitoring program and for informing the public about radioactivity and radiation protection.

Already in 1959 a first automatic aerosol sampling station with an on-line measurement of the beta radioactivity of the aerosols was installed at the Jungfrauoch research station. The advantage of a sampling station at high altitude is that radioactive air masses coming from atmospheric nuclear weapon tests outside Switzerland can be detected more easily and faster than in the ground level air. So, for example (see figure 1.1) the first French nuclear weapon test, performed in February 13th 1960 (60 kT) in Reggane (Sahara/Algeria; Algeria was a French Department until July 5th 1962) could be easily detected at the Jungfrauoch. The activity was almost one order of magnitude higher than at the sampling station in Locarno. These samplers have been replaced starting from 1994 (2001) by a more modern type of sampler that is part of nationwide network of 11 stations (RADAIR).

The RADAIR data (gross alpha and gross beta activity) are transmitted every 30 minutes to a data center in Fribourg. Artificial (net) beta radioactivity is calculated by a mathematical algorithm, with a detection limit of a few tenths of a Bq/m³. Until 2006 only gross beta and/or gross alpha radioactivity was measured at Jungfrauoch. The present work reports on the test of a Digital High Volume Sampler with an air flow of up to 60 m³/h that will allow laboratory analysis of the filters by High Resolution Gamma Spectroscopy.

2 Radioactivity

The stability or instability of a given nuclide is determined by the ratio of its protons and neutrons. Heavy nuclei have a n/p ratio of approximately 1.4. If now either the number of neutrons is too important or the number of protons too small the nuclei are unstable and will transform into a stable one. The largest part of the nuclides is unstable and called radioactive nuclides. Radioactivity is characterized by the spontaneous transformation of unstable atomic nuclei under delivery of energy in form of ionizing α -, β - and γ -radiation, which proceeds directly from the atomic nucleus. The transition to a stable nuclide can either be directly or take place in form of many transformations over several unstable intermediate stages. There are different types of radioactive transformation resp. radioactive decay. One differentiates α - and β -decay, electron capture (EC) and γ -transition. Details are given in section 2.3.

2.1 Laws

The spontaneous transformation of radioactive nuclides is a statistical procedure. The probability to decay of a certain nucleus is independent of its age and each nucleus of the same isotope has the same decay probability. The moment in time a nucleus decays is therefore unknown. However if the number of radioactive isotopes is high one can say how many transformations happen in average in a certain time interval. If at time t a substance contains N atoms of a radioactive nuclide, then the average number of transformations in an interval dt is given by 2.1

$$dN = -\lambda N dt \quad (2.1)$$

λ is the decay constant which is characteristic for every isotope and is a measure for the decay probability. $[\lambda] = [s^{-1}]$. If one integrates equation 2.1 one gets a function which shows the exponential decay of radioactive nuclides.

$$\int_{N(0)}^{N(t)} \frac{dN}{N} = - \int_0^t \lambda dt \quad (2.2)$$

$$\ln N(t) - \ln N(0) = -\lambda t \quad (2.3)$$

$$N(t) = N(0)e^{-\lambda t} \quad (2.4)$$

$N(0)$ is the number of radioactive atoms at $t = 0$ and $N(t)$ the remaining number after a certain time t . Thus of initially $N(0)$ atoms $\Delta N = N(0) (1 - e^{-\lambda t})$ decay in average

in the period $[0, t]$. Therefore always the same fraction of atoms decay in the same time periods. The time $\tau = \frac{1}{\lambda}$ designates the mean lifetime of a nucleus and is the time until the number $N(0)$ decreases to $\frac{N(0)}{e}$. The more common way to express lifetimes is the concept of half-life $T_{1/2}$. This is the time during which the initial number of radioactive isotopes is halved.

$$T_{1/2} = \tau \ln 2 = \frac{\ln 2}{\lambda} = \frac{0.6931}{\lambda} \quad (2.5)$$

Activity The number of radioactive nuclei cannot be measured directly. One can only determine the rate of transformation called the activity by measuring the particles emitted. It is proportional to the number of atoms

$$A = \frac{dN}{dt} = -\lambda N \quad (2.6)$$

The activity represents the number of disintegrations per second and it is measured in Becquerel Bq. $[\text{Bq}] = [\text{s}^{-1}]$. One has to be careful and not confound it to a frequency, which is measured in Hertz $[\text{Hz}] = [\text{s}^{-1}]$. The old unit of activity was Curie Ci and represented the activity of 1g of Radium-226. $1\text{Ci} = 3.7 \cdot 10^{10}\text{Bq}$.

2.2 Radioactive equilibrium

In a radioactive decay the produced nuclei are often radioactive themselves. Such continued radioactive transformation processes lead to whole decay chains. The genetically following nuclides are called mother and daughter nuclides etc. Radioactive nuclides in genetic connection do not follow any longer the simple exponential transformation law for the temporal reduction of the activity. In a radioactive chain the number N_i of the i^{th} nuclide depends on its proper decay ($-\lambda_i N_i$) and on the production coming from its mother nuclide. The production can be described by a function $q_i(t)$ (source: [3]). The temporal variation of the atomic number $N_i(t)$ is given by equation 2.7

$$\frac{dN_i(t)}{dt} = q_i(t) - \lambda_i N_i \quad (2.7)$$

Integration of 2.7 leads to

$$N_i(t) = \left[N_i(0) + \int_0^t q_i(t) e^{\lambda_i t} dt \right] e^{-\lambda_i t} \quad (2.8)$$

In the same way one can calculate the number of the next species of nuclide if $N_i(t)$ of equation 2.8 is known. With $q_{i+1}(t) = \lambda_i N_i(t)$ the solution for the number $N_{i+1}(t)$ is

$$N_{i+1}(t) = \left[N_{i+1}(0) + \int_0^t \lambda_i N_i(t) e^{\lambda_{i+1} t} dt \right] e^{-\lambda_{i+1} t} \quad (2.9)$$

The simple exponential law 2.1 for radioactive decay is a consequence of 2.8 if one sets $q_i(t) = 0$.

Secular equilibrium The case of the transformation of a very long-lived parent nuclide $T_{1/2(1)}$ into a short-lived daughter nuclide $T_{1/2(2)}$ with $T_{1/2(1)} \gg T_{1/2(2)}$. The activity of the mother nuclide does not change consequently and guarantees a constant production of its daughter nuclide during a long time. With equation 2.8 one calculates the number of atoms of the daughter nuclide

$$q_2(t) = \lambda_1 N_1 = A_1 \quad (2.10)$$

$$N_2(t) = \frac{A_1}{\lambda_2} + \left[N_2(0) - \frac{A_1}{\lambda_2} \right] e^{-\lambda_2 t} \quad (2.11)$$

The activity of the daughter nuclide increases exponentially in time and for $t \rightarrow \infty$ equilibrium is reached.

$$N_2(\infty) = \frac{A_1}{\lambda_2}; \quad A_2(\infty) = A_1 = A_1(0)e^{-\lambda_1 t} \quad (2.12)$$

In practice equilibrium is already reached after 6 half-lives of the daughter nuclide. In radioactive equilibrium the activities of mother and daughter nuclide are equal, not to confound with the number of atoms. As an example: The isotope ^{222}Rn of the noble gas radon ($T_{1/2} = 3.825d$) is a daughter nuclide of ^{226}Ra ($T_{1/2} = 1600y$) and secular equilibrium is reached after 23 days.

Current equilibrium If the half-life of mother nuclide is shorter than the one of its daughter nuclide one cannot neglect the decreasing activity of the mother nuclide. The production of the daughter nuclide follows the exponentially decreasing mother nuclide.

$$q_2(t) = \lambda_1 N_1(0)e^{-\lambda_1 t} \quad (2.13)$$

With the initial condition $N_2(0) = 0$ equation 2.8 leads to the general solution

$$N_2(t) = \frac{\lambda_1}{\lambda_2 - \lambda_1} N_1(0) \left[e^{-\lambda_1 t} - e^{-\lambda_2 t} \right] \quad (2.14)$$

For the case of a short lived mother nuclide in comparison to a longer lived daughter nuclide, i.e. $T_{1/2(1)} \ll T_{1/2(2)}$, the mother nuclide will disappear long before its daughter nuclide as $e^{-\lambda_1 t} \rightarrow 0$ equation 2.14 reduces to

$$N_2(t) \cong \frac{\lambda_1}{\lambda_1 - \lambda_2} N_1(0)e^{-\lambda_2 t} \quad (2.15)$$

In order to get the respective activities, we need to multiply both sides by λ_1 and λ_2 and take into account, that $\lambda_1 \gg \lambda_2$ to get the final result

$$A_2(t) \cong A_1(0) \frac{\lambda_2}{\lambda_1} e^{-\lambda_2 t} \quad (2.16)$$

2.3 Decay modes [1]

2.3.1 Alpha decay

In alpha decay an unstable nucleus disintegrates into a lighter nucleus and an alpha particle. An alpha particle consists of two protons and two neutrons and is therefore the same as a stable helium nucleus ${}^4\text{He}$. For energetic reasons α -decay happens only for heavy nuclides with $A > 170$ and $Z > 70$ according to



where X and X' are different elements. Decay processes of this kind liberate energy, since the decay products are more tightly bound than the initial nucleus. The liberated energy which appears as the kinetic energy of the alpha particle and the daughter nucleus X' can be found from the masses of the nuclei involved:

$$Q = [m(X) - m(X') - m({}^4\text{He})] c^2 \quad (2.18)$$

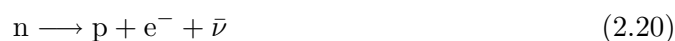
Typical alpha decay energies are a few MeV; thus the kinetic energies of the alpha particle and the nucleus are much smaller than their corresponding rest energies, and so we can use nonrelativistic mechanics to find the energy of the alpha particle:

$$K_\alpha \cong \frac{A-4}{A} Q \quad (2.19)$$

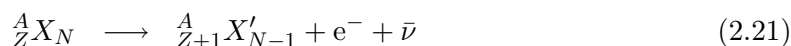
The alpha decay is a proof of quantum tunneling: The Coulomb barrier of the nucleus would be too high for the alpha particle to escape if it couldn't borrow a necessary amount of energy ΔE out of the uncertainty relationship $\Delta E \cdot \Delta t \sim h$ for an infinitesimal time Δt where h is Planck's constant.

2.3.2 Beta decay

In a beta decay a neutron in the nucleus changes into a proton (β^- -decay) or a proton changes into a neutron (β^+ -decay). Z and N each change by one unit but A does not change. First the emitted particles were called beta particles; later they were shown to be electrons or positrons. The emitted electron is not one of the orbital electrons of the atom. The electron is produced by the nucleus out of the available energy. If the rest energy difference between the nuclei is at least $m_e c^2$, this will be possible. Due to conservation laws and to the continuous energy spectrum of the emitted electrons there must be another particle going out of beta decay sharing its energy. Pauli postulated in 1930 a third neutral particle because charge was already conserved. The new particle was called neutrino and is part of the lepton family in the standard model. The complete β^- -decay process is thus



where a free neutron is unstable in contrary to a proton. In the standard model every particle has an antiparticle and $\bar{\nu}$ is called antineutrino. Neutron decay can also occur in a nucleus, in which a nucleus with Z protons and N neutrons decays to a nucleus with $Z+1$ protons and $N-1$ neutrons:

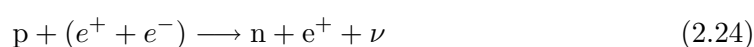


$$Q = [m({}^A X) - m({}^A X')] c^2 \quad (2.22)$$

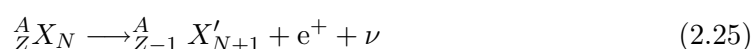
The energy released in the decay appears as the energy E_ν of the antineutrino, the kinetic energy of K_e of the electron, and a small and usually negligible kinetic recoil energy of the nucleus X' .

$$Q \cong E_\nu + K_e \quad (2.23)$$

Another beta decay process is the so called β^+ -decay in which a positron is emitted.



The positron is the antiparticle of the electron. The only change of an antiparticle is its charge. The β^+ -decay is only possible if the available energy is greater than 1 MeV in order to produce the electron-positron pair ($E \geq 2 \cdot m_e c^2$). This decay has a negative Q value because the neutron mass is higher than the proton mass and so it is never observed in nature for free protons. And this is indeed fortunate, if the free proton were unstable to beta decay, stable hydrogen atoms, the basic material of the universe, could not exist! Protons ($T_{1/2} \geq 10^{30}y$) in nuclei can undergo such decay processes:

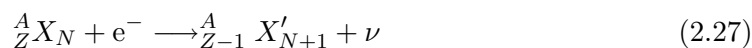


2.3.3 Electron capture EC

A nuclear decay process that competes with positron emission is electron capture. It can also be considered as a beta decay if the available energy is too small for β^+ . The basic electron capture process is



in which a proton captures an electron from its orbit and converts into a neutron plus a neutrino. The electron necessary for this process is one of the innermost K-shell electrons in an atom. The electron capture process does not occur for free protons, but in nuclei the process is



2.3.4 Gamma transition

Following alpha or beta decay, the final nucleus may be left in an excited state. Just as an atom does, the nucleus will reach its ground state after emitting one or more photons, known as nuclear gamma rays. The energy of each photon or the sum of the energies in gamma-cascades is the energy difference between the initial and final nuclear states, less a negligibly small correction for the recoil kinetic energy of the nucleus. These energies are typically in the range of 100 keV to a few MeV and are thus highly ionizing radiations.

2.4 Natural Radioactivity

All of the elements beyond the very lightest hydrogen were produced by nuclear reactions in the interiors of stars. These reactions produce not only stable elements, but radioactive ones as well. Above lead (Pb $Z=82$) no more stable isotopes do exist. Most of the radioactive elements have half-lives of the order of days or years, much smaller than the age of the Earth (about $4.5 \cdot 10^9 y$). Therefore, most of the radioactive elements that may have been present when stars and the Earth were formed have decayed to stable elements. However a few of them have half-lives of the order as the age of the Earth, and so are still present. Those radioisotopes represent the natural radioactivity. Artificial radioactivity consists of manmade radioactive isotopes these are especially the fission products of heavier nuclei produced in atomic bombs, nuclear power plants and particle accelerators.

Radioactive material is found throughout nature. It occurs naturally in the soil, rocks, water, air, and vegetation. 76 different natural radioactive isotopes are known today, the largest part of it lies in the 4 natural decay series. These are the thorium series, uranium series, neptunium series and actinium series (or uranium-235 series). The neptunium series, starting with ^{237}Np , does not exist anymore because of the shorter half-life of $2.1 \cdot 10^6$ years of Neptunium compared to the age of the earth all the isotopes in this series have decayed.

Table 2.1: Thorium series $A=4n$. The three bold written isotopes are the ones measured by gamma spectrometry in our experiments.

Nuclide	Decay	$T_{1/2}$	MeV	Product
^{232}Th	α	1,405·10 ¹⁰ a	4,083	^{228}Ra
^{228}Ra	β^-	6,7 a	1,325	^{228}Ac
^{228}Ac	β^-	6,15 h	2,127	^{228}Th
^{228}Th	α	1,9131 a	5,520	^{224}Ra
^{224}Ra	α	3,66 d	5,789	^{220}Rn
^{220}Rn	α	55,6 s	6,405	^{216}Po
^{216}Po	α	0,145 s	6,906	^{212}Pb
^{212}Pb	β^-	10,64 h	0,574	^{212}Bi
^{212}Bi	β^- 64,06 % α 35,94 %	60,55 min	2,254 6,207	^{212}Po ^{208}Tl
^{212}Po	α	2,99·10 ⁻⁷ s	8,954	^{208}Pb
^{208}Tl	β^-	3,083 min	5,001	^{208}Pb
^{208}Pb	.	stable	.	

Figure 2.1: Thorium series. Left arrows represent α -decay and right arrows β^- -decay. Source [26]

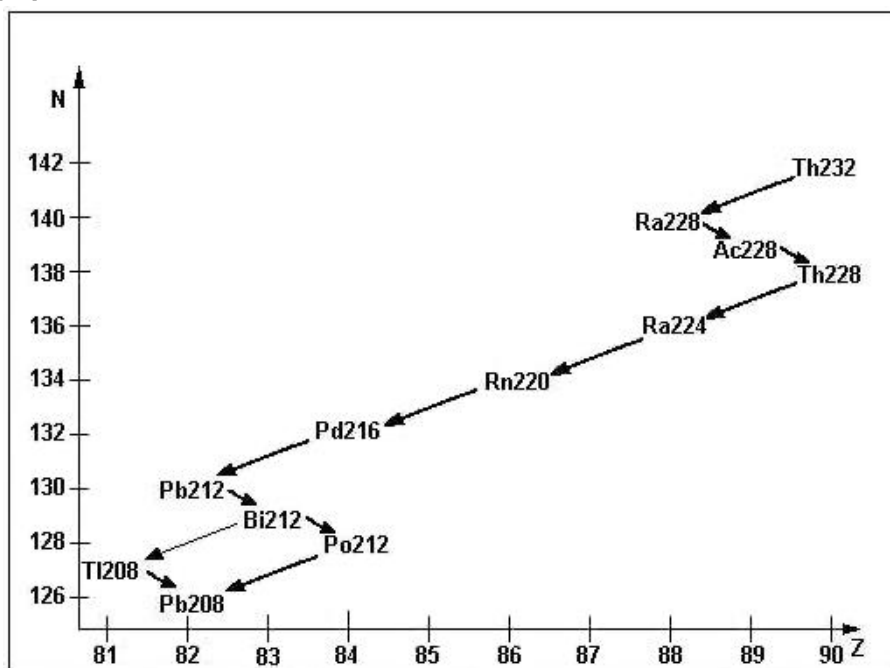


Table 2.2: Uranium series $A=4n+2$. The radioisotopes measured by γ -spectroscopy are ^{214}Pb , ^{214}Bi and ^{210}Pb

Nuclide	Decay	$T_{1/2}$	MeV	Product
^{238}U	α	$4,468 \cdot 10^9$ y	4,270	^{234}Th
^{234}Th	β^-	24,10 d	0,273	^{234}Pa
^{234}Pa	β^-	6,70 h	2,197	^{234}U
^{234}U	α	245500 y	4,859	^{230}Th
^{230}Th	α	75380 y	4,770	^{226}Ra
^{226}Ra	α	1602 y	4,871	^{222}Rn
^{222}Rn	α	3,8235 d	5,590	^{218}Po
^{218}Po	α 99,98 %	3,10 min	6,615	^{214}Pb
	β^- 0,02 %		0,265	^{218}At
^{218}At	α 99,90 %	1,5 s	6,874	^{214}Bi
	β^- 0,10 %		2,883	^{218}Rn
^{218}Rn	α	35 ms	7,263	^{214}Po
^{214}Pb	β^-	26,8 min	1,024	^{214}Bi
^{214}Bi	β^- 99,98 %	19,9 min	3,272	^{214}Po
	α 0,02 %		5,617	^{210}Tl
^{214}Po	α	0,1643 ms	7,883	^{210}Pb
^{210}Tl	β^-	1,30 min	5,484	^{210}Pb
^{210}Pb	β^-	22,3 y	0,064	^{210}Bi
^{210}Bi	β^- 99,99987%	5.013 d	1,426	^{210}Po
	α 0,00013%		5,982	^{206}Tl
^{210}Po	α	138,376 d	5,407	^{206}Pb
^{206}Tl	β^-	4,199 min	1,533	^{206}Pb
^{206}Pb	.	stable	.	

Figure 2.2: Uranium series. Left arrows represent α -decay and right arrows β^- -decay. Source [26]

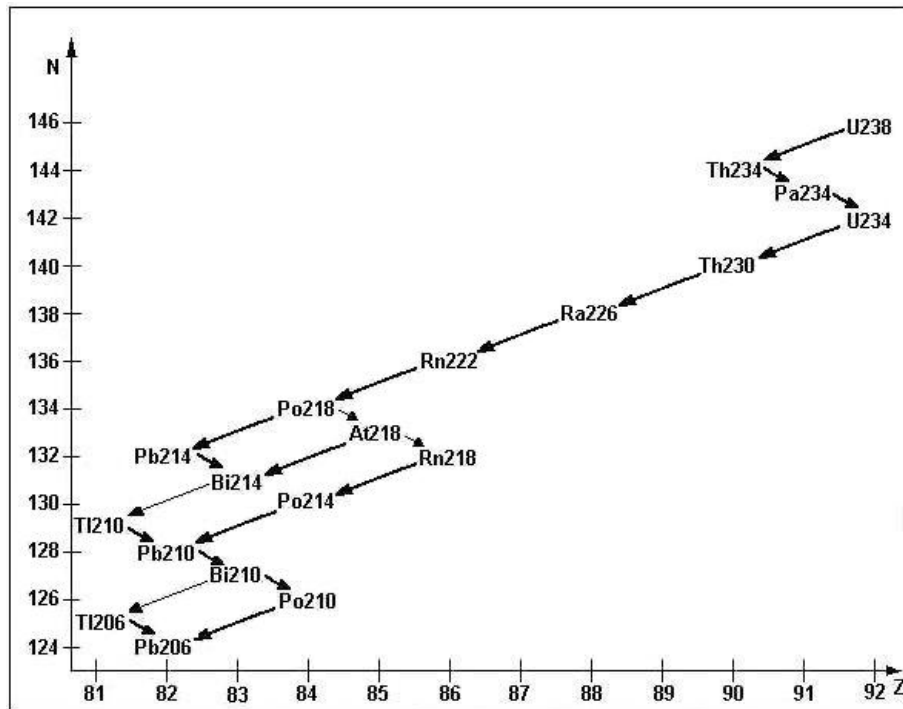


Figure 2.3: Uranium-235 series. Left arrows represent α -decay and right arrows β^- -decay. Source [26]

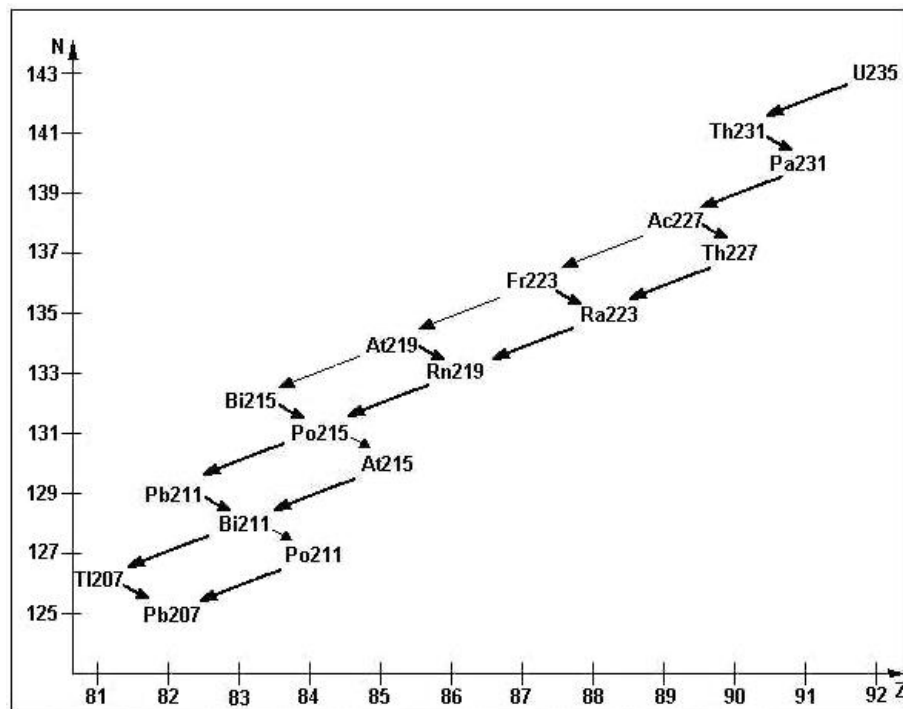


Table 2.3: Uranium-235 series. Uranium 235 is contained in the soil and decays stepwise into the noble gas radon ^{219}Rn but its half-life of 3.96s is too short to ascend into the atmosphere and that's the reason why we do not measure decay products in ambient air. Today's ratio of $^{235}\text{U}/^{238}\text{U}$ is approx. 0.72%. With their corresponding half-lives one can calculate the age of the earth to $4.5 \cdot 10^9$ y.

Nuclide	Decay	$T_{1/2}$	MeV	Product
^{235}U	α	$7,038 \cdot 10^8$ y	4,679	^{231}Th
^{231}Th	β^- α 0,000001 %	25,52 h	0,389 0,389	^{231}Pa ^{227}Ra
^{231}Pa	α	32760 y	5,149	^{227}Ac
^{227}Ra	α	42,2 min	1,325	^{223}Rn
^{227}Ac	β^- 98,62 % α 1,38 %	21,773 y	0,045 5,042	^{227}Th ^{223}Fr
^{227}Th	α	18,72 d	6,146	^{223}Ra
^{223}Rn	β^-	23,2 min	1,000	^{223}Fr
^{223}Fr	β^- 99,994 % α 0,006 %	22,0 min	1,149 5,430	^{223}Ra ^{219}At
^{223}Ra	α	11,435 d	5,979	^{219}Rn
^{219}At	α 99,99 % β^- 0,01 %	56 s	6,390 1,700	^{215}Bi ^{219}Rn
^{219}Rn	α	3,96 s	6,946	^{215}Po
^{215}Bi	β^-	7,6 min	2,250	^{215}Po
^{215}Po	α β^- 0,000023 %	1,781 ms	7,526 0,721	^{211}Pb ^{215}Rn
^{215}At	α	0,10 ms	8,178	^{211}Bi
^{211}Pb	β^-	36,1 min	1,373	^{211}Bi
^{211}Bi	α 99,72 % β^- 0,28 %	2,14 min	0,579 6,751	^{207}Tl ^{211}Po
^{211}Po	α	0,516 s	7,595	^{207}Pb
^{207}Tl	β^-	4,77 min	14,23	^{207}Pb
^{207}Pb	.	stable	.	.

Table 2.4: In the soil and vegetation some other radioactive isotopes are present with very long half-lives and which are not present in decay series. The most important one is the radioactive potassium ^{40}K present in soil and plants. The ratio $^{40}\text{K}/\text{K}=0.012\%$ is constant. Its distribution is very homogeneous and it represents the largest activity in Swiss soils of about 200 Bq/kg. One finds also part of it in milk ($\sim 50\text{Bq/l}$) and it is present in the human body especially in muscles.

Nuclide	Decay	$T_{1/2}$ [y]	Relative abundance (%)
^{40}K	β^- , EC	1.28 E9	0.0128
^{87}Rb	β^-	4.8 E10	27.83
^{115}In	β^-	4.0 E14	95.7
^{130}Te	$2\beta^-$	1.0 E21	33.8
^{138}La	β^- , EC	1.35 E11	0.09
^{144}Nd	α	2.1 E15	23.8
^{147}Sm	α	1.06 E11	15
^{176}Lu	β^-	3.6 E10	2.6
^{174}Hf	α	2.0 E15	0.16
^{187}Re	β^-	5.0 E10	62.6
^{186}Os	α	2.0 E15	1.58
^{190}Pt	α	6.1 E11	0.01
^{204}Pb	α	1.4 E17	1.4

2.4.1 Natural Radioactivity in Air

The air filters we measure contain many daughter nuclides of the two decay series, namely the thorium- and the uranium series. By gamma spectrometry the following isotopes can be measured: ^{214}Pb , ^{214}Bi and ^{210}Pb part of the uranium series and ^{212}Pb , ^{212}Bi , and ^{208}Tl part of the thorium series. In both cases it is a radioactive Radon isotope which can escape from the soil and ascend into the air. The decay products are metal atoms and easily attach to aerosols, which are then collected on our filter samples with the Digital High Volume Air Sampler.

Once the radon is released in the air the decay products of both series are governed by the same meteorological conditions. Mean concentrations of both mother nuclides ^{238}U and ^{232}Th in swiss soil are equivalent of about 25 Bq/kg and this source is assumed to be constant. Considering these facts the activity of all daughter nuclides in ambient air should follow the same variations due to changing meteorological conditions. The biggest difference lies in the half-lives of the radon isotopes: ^{220}Rn has only 55.6 s while ^{222}Rn has 3.82 d. It means that the short lived ^{220}Rn has not enough time to reach appreciable altitudes while ^{222}Rn can be transported to the upper troposphere. This can only partly be compensated by the longer half-lives of ^{212}Pb and ^{212}Bi .

2.4.2 Measurement

In order to get precise data the filters are measured immediately after collection. In general it took some 6-10 minutes to start the measurement. Enough time for three half-lives of ^{218}Po , the mother nuclide of ^{214}Pb . The measured net counts of those isotopes do not represent their real activities in air, because of the decay series. Parts of the measured Bismut isotopes were originally Lead isotopes and so forth.

A special formula for both decay series had to be developed in order to calculate their real activities in air. The basic assumption for the formula is that the daughter nuclides of the same series are in activity equilibrium in the air as well as on the filter. It means that for each isotope there is the same number of disintegrations per second. This can be assumed because of the much longer half-lives of the mother nuclides uranium and thorium.

2.4.3 Calculations

Uranium decay series: The short lived daughter nuclides on the filter are ^{218}Po with $T_{1/2} = 3$ min ^{214}Pb with $T_{1/2} = 26.8$ min and ^{214}Bi with $T_{1/2} = 19.7$ min. During the transfer of the filter to the detector almost all Polonium-218 atoms decay into Lead. As the measuring time of 2 days is much longer than the respective half-lives, we can assume further that all the atoms in the beginning present on the filter have decayed. Thus the measured counts of ^{214}Bi contain all ^{214}Pb and all ^{218}Po counts as the measured ^{214}Pb

contain the ^{218}Po counts. The activity on the filter is in equilibrium, the same number of isotopes get on the filter as do decay per unit of time. $N_{\text{Pb-214}}^*$ and $N_{\text{Bi-214}}^*$ are the calculated number of atoms out of the registered counts of each element. This does not correspond to the real initial number because of the decay of those elements on the filter.

Measured quantities: $N_{\text{Pb-214}}^*$, $N_{\text{Bi-214}}^*$, Q air flow rate [$\frac{m^3}{s}$]

$$A_{\text{Po-218}}(\text{filter}) = \frac{A_{\text{Po-218}}(\text{air})}{\lambda_{\text{Po-218}}} Q \quad (2.28)$$

$$A_{\text{Pb-214}}(\text{filter}) = A_{\text{Po-218}}(\text{filter}) + \frac{A_{\text{Pb-214}}(\text{air})}{\lambda_{\text{Pb-214}}} Q \quad (2.29)$$

$$A_{\text{Bi-214}}(\text{filter}) = A_{\text{Pb-214}}(\text{filter}) + \frac{A_{\text{Bi-214}}(\text{air})}{\lambda_{\text{Bi-214}}} Q \quad (2.30)$$

The activity on the filter is equal to the activity coming from the air plus the activity coming from the mother nuclide already on the filter. And as assumed the activity in the air of all three isotopes is equal one can transform above equations.

$$A_{\text{Pb-214}}(\text{filter}) = \frac{A_{\text{Po-218}}(\text{air})}{\lambda_{\text{Po-218}}} Q + \frac{A_{\text{Pb-214}}(\text{air})}{\lambda_{\text{Pb-214}}} Q \quad (2.31)$$

$$= A_{\text{Pb-214}}(\text{air}) Q \left(\frac{1}{\lambda_{\text{Po-218}}} + \frac{1}{\lambda_{\text{Pb-214}}} \right) \quad (2.32)$$

$$A_{\text{Bi-214}}(\text{filter}) = \frac{A_{\text{Po-218}}(\text{air})}{\lambda_{\text{Po-218}}} Q + \frac{A_{\text{Pb-214}}(\text{air})}{\lambda_{\text{Pb-214}}} Q + \frac{A_{\text{Bi-214}}(\text{air})}{\lambda_{\text{Bi-214}}} Q \quad (2.33)$$

$$(2.34)$$

$$A_{\text{Bi-214}}(\text{filter}) = A_{\text{Bi-214}}(\text{air}) Q \left(\frac{1}{\lambda_{\text{Po-218}}} + \frac{1}{\lambda_{\text{Pb-214}}} + \frac{1}{\lambda_{\text{Bi-214}}} \right) \quad (2.35)$$

The effective number of ^{214}Bi atoms on the filter at the end of sampling is the difference between the measured quantities of ^{214}Bi and ^{214}Pb .

$$N_{\text{Bi-214}}(\text{filter}) = N_{\text{Bi-214}}^* - N_{\text{Pb-214}}^* \quad (2.36)$$

transforming 2.35 leads to the final formula for the activity in air:

$$A_{\text{Bi-214}}(\text{air}) = \frac{\lambda_{\text{Bi-214}} (N_{\text{Bi-214}}^* - N_{\text{Pb-214}}^*)}{Q \left(\frac{1}{\lambda_{\text{Po-218}}} + \frac{1}{\lambda_{\text{Pb-214}}} + \frac{1}{\lambda_{\text{Bi-214}}} \right)} \quad (2.37)$$

$$A_{\text{Bi-214}}(\text{air}) = A_{\text{Pb-214}}(\text{air}) = A_{\text{Po-218}}(\text{air}) \quad (2.38)$$

Pb-210 ^{210}Pb is a long lived daughter nuclide in the uranium chain and follows onto ^{214}Bi . Its half-life is 22.3 years. Due to the half-life of 3.82 days of its predecessor ^{222}Rn it can reach high altitudes in the troposphere, especially in summer when convection is entrained. It follows thus the same scavenging mechanisms as the cosmogenic ^7Be described later. ^{210}Pb emits one single gamma-ray at an energy of 46.5 keV and decays in several steps into the stable ^{206}Pb isotope as listed in table 2.2. Its detection is not always guaranteed because at this low energy the efficiency of the detector is very low and the x-ray background is high leading to poor counting statistics. The activity is calculated with equation 2.43.

Thorium decay series The short lived daughter nuclides on the filter are ^{216}Po with $T_{1/2} = 0.145$ s, ^{212}Pb with $T_{1/2} = 10.64$ h, ^{212}Bi with $T_{1/2} = 60.55$ min and ^{208}Tl with $T_{1/2} = 3.083$ min. During the transfer of the filters to the detector all the ^{216}Po atoms decay. For the thorium series we cannot assume to count all the atoms present on the filter because only 4 half-lives of ^{212}Pb will pass during the usual measuring time of 160 000 s. Thus another formula has to be used:

Measured quantities: $N_{\text{Pb-212}}$ calculated number of ^{212}Pb atoms out of the registered peak net area (2.43).

$$N_{\text{Pb-212}} = \int_{T_1}^{T_2} A(t) dt = \lambda_{\text{Pb-212}} N_1 \int_{T_1}^{T_2} e^{-\lambda_{\text{Pb-212}} \cdot t} dt \quad (2.39)$$

For T_1 being the starting time of the measurement and T_2 being the end of the measurement (in general $T_2 = 160'000\text{s}$). N_1 is the number of atoms present on the filter at time T_1 . We are interested in the number N_0 of atoms present on the filter at the moment of filter change at time T_0 . In order to calculate this we need the transfer time $\Delta T = T_1 - T_0$ and extract N_1 in above equation 2.39.

$$N_1 = \frac{N_{\text{Pb-212}}}{\lambda_{\text{Pb-212}} \int_{T_1}^{T_2} e^{-\lambda_{\text{Pb-212}} \cdot t} dt} \cong 1.0585 \cdot N_{\text{Pb-212}} \quad (2.40)$$

$$N_0 = N_1 \cdot e^{\lambda_{\text{Pb-212}} \cdot \Delta T} \quad (2.41)$$

Now as for the uranium chain this number contains also all the atoms first being Polonium atoms, we can use again the same principles of equilibrium and write for the final formula:

$$A_{\text{Pb-212}}(\text{air}) = \lambda_{\text{Pb-212}} \cdot N_0 \cdot Q^{-1} \left(\frac{1}{\lambda_{\text{Po-216}}} + \frac{1}{\lambda_{\text{Pb-212}}} \right)^{-1} \quad (2.42)$$

Longer lived natural radionuclides For the longer lived radionuclides such as ^7Be , ^{210}Pb , ^{40}K and ^{137}Cs ($T_{1/2}=30$ y) we use a simpler formula. The calculated activities on the filters at the very end of sampling are based on the determined peak net area F_i provided by the software InterWinnerTM described in subsection 5.6.1 and a decay correction and lead to the formula:

$$A_i = \frac{F_i}{\gamma_i \epsilon_i} \lambda_i \frac{t_r}{t_l} \frac{e^{\lambda_i \Delta T}}{1 - e^{-\lambda_i t_r}} \quad (2.43)$$

Where γ_i is the emission probability, ϵ_i the efficiency of the detector at the respective energy, t_r and t_l the real and live time of the detector and ΔT is the time between the end of sampling and the beginning of measurement. For Beryllium one has to take into account disintegration during sampling. Therefore the activities are back calculated to the middle of the sampling interval. The concentrations in air are calculated with a normalized volume i.e. at pressure 1013 hPa and a temperature of 288 K. Thus the measurements can be better compared.

3 Atmosphere

The word atmosphere originates from the Greek *atmos* = vapor and *sphaira* = sphere and designates the gas covering held by the terrestrial attraction force around the globe. It consists mainly of the gases nitrogen (78.09 %), oxygen (20,95 %), argon (0,93 %) and carbon dioxide (0,03 %). The atmosphere possesses no defined upper limit and is drawn by an exponential dilution with increasing height, this leads to a vertical structure with pronounced temperature distributions. One differentiates between troposphere, stratosphere, mesosphere, thermosphere and exosphere. A schematic picture is given in figure 3.1.

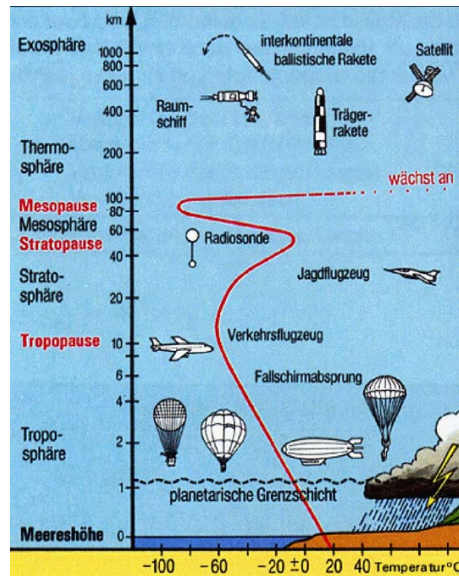
3.1 Troposphere

The troposphere forms the lowest layer of the atmosphere and has an upper limit from 8 to 15 km, depending upon geographical latitude and weather conditions. This difference is released by the vertical movements of air in the troposphere. The heating up of the earth's surface by the sun and the backscattering of this warmth to air leads to convection and to a middle temperature decrease at a value of $6.5\text{ }^{\circ}\text{C}/\text{km}$. In the planetary boundary layer high up to 2.5 km the influence of the earth's surface causes strong changes of temperature, wind and humidity. Here layers do exist, in which the temperature increases with increasing height . One speaks here of inversions. The troposphere contains approximately 80% of the entire mass of the atmosphere and is therefore the closest part of it. The very most weather phenomena take place in this layer, because here also nearly the entire water vapour is contained of the atmosphere. The upper limit of the troposphere is characterized by a temperature inversion, which prevents any vertical movement of air. One calls this border the tropopause. In figure 3.1 this change in temperature is clearly seen at an altitude of 10 km. The tropopause can suddenly disappear and reappear at a different altitude and in the case of shifting upwards leaving stratospheric air in the troposphere called stratospheric intrusions.

3.2 Stratosphere

The stratosphere expands from the end of the troposphere at a value of approximately 50 km and is drier than the troposphere and also much thinner. With rising height the stratosphere warms up to a maximum reached by approximately -3°C . The long-wave UV

Figure 3.1: Nomenclature and temperature profile of earth's atmosphere. Source: Fonds der Chemischen Industrie Folienserie: Umweltbereich Luft 1987



radiation splits oxygen molecules O_2 , these fragments react with further oxygen to ozone O_3 . In this way a global ozone veil at a height of 25-45 km is developed, which absorbs again a large part of the dangerous UV light. This UV absorption is an exothermic process and therefore warms up the stratosphere and temperature increases.

3.3 Mesosphere

The mesosphere is again characterized by a temperature decrease with rising height. It expands from the upper limit of the stratosphere to 85 km. The temperature decreases to -93°C . The components absorb further radiation, are however too little dense to convert this energy into warmth.

3.4 Thermosphere

The thermosphere expands to 600 km, where the temperatures can reach up to 1750°C , if the region is turned towards the sun. In this layer one finds most satellites. UV or more highly energetic radiation can ionize the still existing molecules and produce polar lights in polar regions where the magnetic field is almost perpendicular to earth's surface and therefore cosmic particle can enter the atmosphere. Polar lights increase in frequency every 11 years due to rising solar activity.

3.5 Aerosols

Aerosols are suspensions of firm or liquid particles in air of the order of magnitude nanometer to some micrometers. Aerosols can be due to natural or human sources. In addition one differentiates between primary and secondary sources. With the primary the particles arrive directly into the atmosphere and with the secondary they are only formed in air out of gas molecules. Such gases are nitrogen oxides NO_x , sulfur dioxide SO_2 and hydrocarbons. One mostly characterizes the aerosols by their geometrical diameters D and divides them into two large classes: One calls the particles "rough" if D is 1-2 μm and "fine" if it is smaller. The rough aerosols originate particularly from erosion processes and are brought by the wind into the atmosphere. In addition particles of this order of magnitude are pollen and bacteria. Due to their size and their weight they sedimentate quite fast by dry deposit see figure 3.2. The natural aerosols originate from predominantly three sources: mineral dust, sea salts and volcanic emissions.

The sea salt aerosols result from wind and waves when bubbles are bursting, thus sea water droplets can evaporate and inorganic aerosols arrive into the air. Those are mainly the different salts (NaCl contained in the sea water, KCl , CaSO_4 , Na_2SO_4). The size amounts to an average of $8\mu\text{m}$ and the life span is shortened therefore. Mineral-dust arrives from deserts and other dry regions by the wind into air. Particles with diameters of about 10 to 200 μm are usually grains of quartz and if the diameter is below 10 μm it is loam, which consists of oxides or carbonates.

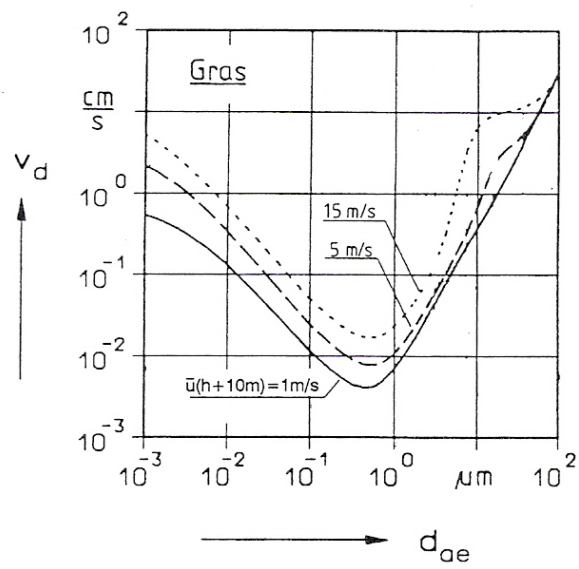
With volcanic eruptions ash, consisting of SiO_2 , Al_2O_3 and Fe_2O_3 arrives into the atmosphere. Additionally gases (SO_2 , H_2S , CO_2) reach the atmosphere from which again aerosols develop in further steps. Particularly long-lived is SO_2 , which can reach the stratosphere and form sulfuric acid H_2SO_4 aerosol droplets.

Aerosols from human source come from the burn of biomass and from industrial processes, these again to a large extent from the production of primary energy carriers, like in mines and oil refineries. With the burn of fossil sources of energy the soot makes a further contribution. From this burn produced gases become secondary sources of aerosol, this concerns especially sulfates and nitrate. The sulfate emissions produced annually by humans are even larger than the natural output.

Aerosols are responsible for the condensation of water vapour as condensation nucleus the building mechanism of clouds and play therefore an important role in earth's radiation budget by changing the atmospheric albedo.

The sedimentation velocity of aerosols on surface objects depends on the aerosol-diameter and is in the range of 0.5 mm/s to cm/s as drawn in figure 3.2

Figure 3.2: Sedimentation velocity on grass depending on the aerosol diameter. Source [12]



4 Cosmic rays

Cosmic rays are highly energetic particles originating from far away galaxies, supernovae, pulsars and last but not least the sun. Solar energetic particles (SEP) and galactic cosmic rays (GCR) cover an energy range of $10 - 10^4$ MeV for the SEP and $10^4 - 10^{14}$ MeV for the GCR([7]). The GCR flux is isotropic whilst this is not the case for SEP.

Cosmic rays were discovered in the beginning of the 20th century by ionization experiments in balloon flights. Albert Gockel former professor of the University of Fribourg was one of the leading physicians in this field of research. He carried out experiments in the years 1909/11. But it was austrian F.V.Hess who received the Nobel Prize for the discovery of cosmic rays in 1936. He was the first to establish quantitative measurements in the years 1910/13.

One differentiates primary and secondary cosmic radiation. Primary radiation consists in 85 % of protons, 14 % in He-nuclei and only a small fraction consists of heavier nuclei up to $Z=30$. Secondary radiation is produced in interaction with earth's atmosphere and its intensity is a function of geographic latitude due to earth's non uniform magnetic field. Cosmic radiation is most intense at the poles and least in equatorial regions. n , p , e^+ , e^- , π , μ , ν , γ are the main constituents of the secondary radiation. Interactions of protons and neutrons with atmospheric O_2 and N_2 can lead to spallation reactions or neutron capture. The radioactive 3H , 7Be and ^{10}Be are spallation products or in other words debris of the N_2 and O_2 molecules. Radio Carbon ^{14}C is a result of neutron capture:



Cosmic radiation undergoes the 11 year cycle of solar activity. Approximately every 11 years the sunspot number is maximum what leads to an increase of solar wind and to a decrease of the total cosmic ray intensity on earth's surface. The bigger flux of solar energetic particles modifies the magnetic field and decreases the intensity of galactic cosmic rays (Forbush Effect). As an example the difference in the 7Be production between the sunspot minimum and maximum is 70 % in the polar region above 14 km in altitude and 7 % in the lower equatorial atmosphere [7].

The contribution of cosmic rays to the external radiation exposure increases with altitude and can be estimated for Switzerland using the following empirical formulas [19]:

$$E_c(z) = E_c(0)e^{0.38z} \quad (4.2)$$

$$E_n(z) = E_n(0)e^{0.78z} \quad (4.3)$$

$E_c(z)$ is the altitude dependent ionizing component of the cosmic radiation whilst $E_n(z)$ is the neutron component, z is the altitude in km, $E_c(0) = 0.24$ mSv/year is the annual dose due to charged particles at sea level and $E_n(0) = 0.066$ mSv/year is the annual dose due to the interactions with neutrons where Sievert Sv is the unit for doserates and corresponds to the absorbed energy per unit of mass [Sv]=[J/kg]. Neutrons contribute to indirect ionizations in the human body especially for neutron capture where β -decays and γ -transformations are a direct consequence.

4.1 Production of beryllium 7 and beryllium 10 radio nuclides

As mentioned before ^7Be and ^{10}Be are spallation products of the interaction of protons and neutrons with atmospheric oxygen and nitrogen. Yoshimori [7] calculated that GCR-produced ^7Be peaks around 20 km in altitude and decreases exponentially with altitude. Galactic cosmic rays produce ^7Be at nearly constant rate while solar energetic particles produce it in association with intense solar proton events. The frequency of intense solar proton events is less than a few events a year. The cross section of p-N reaction peaks at 20 MeV and is almost constant above 40 MeV see figure 4.2. GCR incident on the top of the atmosphere consists of protons with energies around 1 GeV. The characteristic feature of nuclear interactions at these energies is the development of this cascade process. On the way through the atmosphere the radiation loses energy and the molecular density increases thus one expects that the production rate begins to increase at the top of the atmosphere, reaches a maximum at altitudes between 12-16 km depending on nuclide and latitudes and finally decreasing gradually down to the earth's surface. The secondary neutron flux is larger by almost 2 orders of magnitude and reaches its maximum in altitudes of 14.5-17.5 km. Secondary neutrons with energies above 20 MeV much contribute to production of ^7Be in stratosphere. SEP are in the range of 1-100 MeV and because of their relatively low energies nuclear reactions are only produced on top of the atmosphere and near the poles. The long term average production of cosmogenic nuclei by SEP is not expected to be significant. The global ^7Be production rate depends on the number of atoms for target nuclei, the energy-dependent cross section for the production of ^7Be and the total flux of ^7Be producing particles as a function of geomagnetic latitude and atmospheric depth.

4.1.1 Stratosphere to Troposphere Exchange [4]

Beryllium production peaks in an altitude of 20 km in the stratosphere which extends from about 12 km – 50 km. 70 % of the whole production takes place in the stratosphere and only 30 % in the troposphere. Due to the different temperature profiles residence times of aerosols are very different in troposphere and stratosphere. The mean residence time in the troposphere is 10-35 days while it is 1-2 years in the stratosphere. Wet

Figure 4.1: Energy distribution of galactic cosmic ray- and solar protons at a large SEP event on Oct. 28, 2003. Source [8].

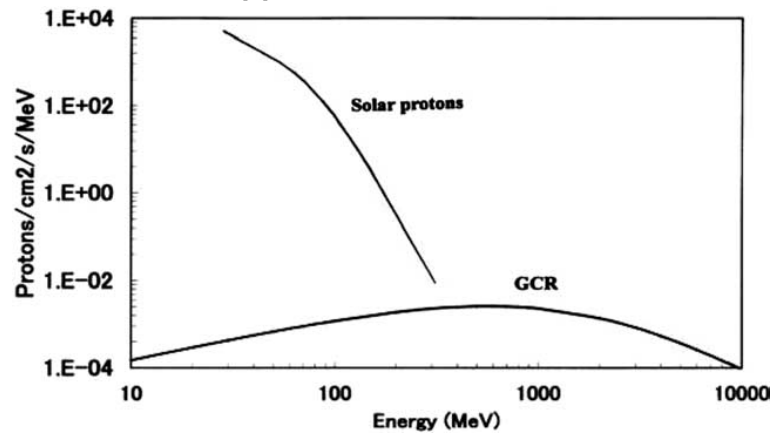
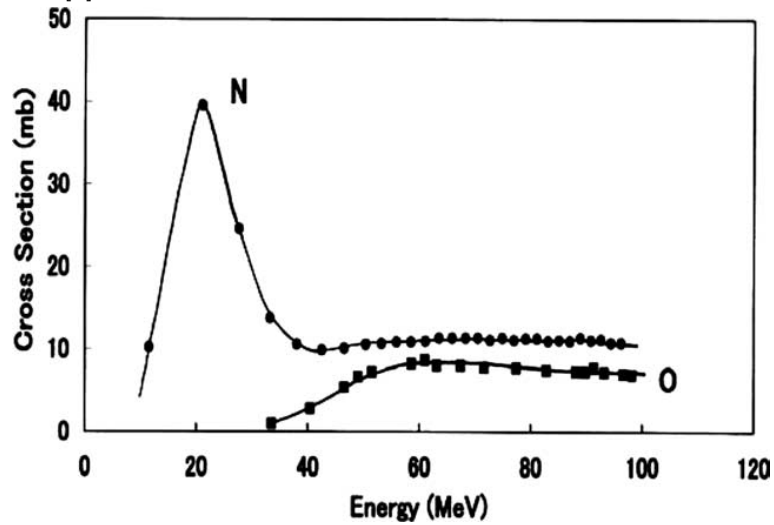


Figure 4.2: Cross sections for ^7Be production from proton-Oxygen and proton-Nitrogen reactions. Source [8].



scavenging is the main process washing tropospheric aerosols out. ^7Be and ^{10}Be are two different radioactive isotopes and have very different half-lives. ^7Be disintegrates by a 477.6 keV gamma emission to the stable Lithium and has 53.3 days as half-life. ^{10}Be is also a β -emitter and very long lived with its 1.5×10^6 years. The average production of those isotopes is not exactly the same due to different cross sections. It was calculated that the ratio of produced Beryllium isotopes $^{10}\text{Be}/^7\text{Be}$ lies between 0.35-0.4 in stratosphere and 0.53-0.6 in the troposphere depending the altitude and geographic latitude (Nagai [17] [2000]). But even at high latitudes a ratio above 1 was never observed. Beryllium isotopes rapidly attach to aerosols and because of the very different half-lives the ratio will rapidly increase in the stratosphere as the aerosols age, where the residence time is much longer than the half-life of ^7Be thus the number of atoms rapidly decrease in comparison to the number of ^{10}Be atoms. The short residence time in the troposphere is insufficient to allow the $^{10}\text{Be}/^7\text{Be}$ ratio to increase appreciably above its production ratio. Transport models showed $^{10}\text{Be}/^7\text{Be}$ ratios up to 8 Between 20-40 km in the stratosphere and generally about 2 near the tropopause. In spring and summer the ratio tends to increase in the lower stratosphere because of descending stratospheric overworld air. Tropopause folds can occur near the jet stream and stratospheric air enters the troposphere the contrary of course happens at the same time making the lower stratosphere a transition layer between the troposphere and the stratospheric overworld. Generally the jet stream is stronger in winter and exchange between the stratospheric overworld and the lower stratosphere is suppressed. This is one reason why Beryllium concentrations on earth's surface are the lowest in winter. Measurements made by Zanis et al. [10] at Jungfaujoch in the year 2000 showed a clear seasonal cycle of the $^{10}\text{Be}/^7\text{Be}$ ratio with a peak in May and June and a minimum in autumn. The values were contained between 1.5 and 3 with an annual mean of 1.97. They showed that the ratio is independent of wet scavenging, meaning that both isotopes are attached to the same kind of aerosols and washed out in the same way. The highest values were associated with cyclonic conditions and northerly advection, which are both typical for stratospheric intrusions.

4.1.2 Seasonal variations in surface-air beryllium concentrations

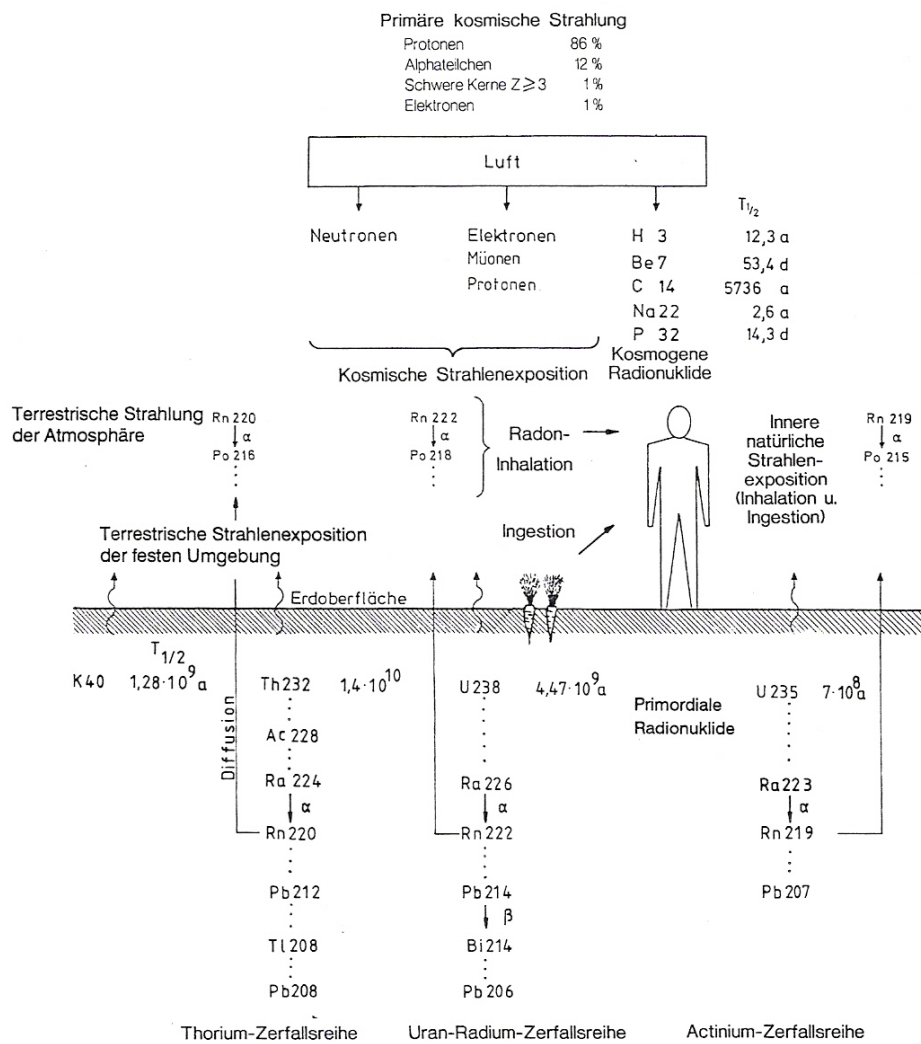
Beryllium concentrations in surface air are the lowest in winter months and usually peak in summer. There are different reasons, some of them are mentioned above. Vertical mixing in the troposphere is largest in summer when the sun is heating the surface and convection is entrained. In this way air from the upper troposphere with higher concentrations is forced downward. The rate of exchange between troposphere and stratosphere is also enlarged in summer bringing air with bigger beryllium concentrations down. Measurements taken in Polar Regions (Feely 1989 [6]) show peak concentrations in winter suggesting horizontal transport of air from middle latitudes to high latitudes. This and the fact that due to stronger jet stream exchange between the stratospheric overworld and the lower stratosphere is suppressed would explain the lows in our region in winters.

4.2 Radioactivity in air

As already described in section 2.4.1 the gamma emitting radon daughter nuclides such as ^{214}Pb , ^{214}Bi , ^{210}Pb , ^{212}Pb , ^{212}Bi , ^{208}Tl contribute to direct radiation and to inhalation. Additionally the cosmogenic radionuclides produced in the atmosphere as ^3H , ^7Be , ^{10}Be , ^{14}C , ^{22}Na are present in air. The higher the altitude the higher the cosmic radiation, also concerning the particles created in the so called secondary radiation: Neutrons, electrons, pions, muons and gamma cascades are part of this secondary radiation attenuated by the atmosphere and lowest in intensity in the equatorial boundary layer.

Two other nuclides frequently measured are ^{40}K and ^{137}Cs . Potassium ^{40}K is in the soil and can be suspended and ascend into the atmosphere. This effect is usually the largest in summer when farmers plow the soil. Same mechanisms are responsible for the resuspension of ^{137}Cs liberated in the 1986 nuclear reactor accident in Chernobyl. Other mechanisms are wood fires liberating ^{137}Cs stored in trees and firs. Thus the ratio of both nuclides can be a tracer of new injected ^{137}Cs . The ^{40}K concentration usually increases in the beginning of August and at the end of the year in Switzerland due to 1st of August and New Years Eve fireworks. Further part of ^{137}Cs is still remaining in the stratosphere as a result of nuclear bomb tests of the 50^{ies} and 60^{ies}. This amount decreases due to less testing see figure 1.1 and due to the half-life of 30 years of ^{137}Cs .

Figure 4.3: Direct and indirect radiation in ambient air. Summary of the major parts of ambient radiation: The daughter nuclides of the uranium and thorium decay series ascending into the atmosphere and the cosmogenic radionuclides and secondary radiation coming from above. Source [12]



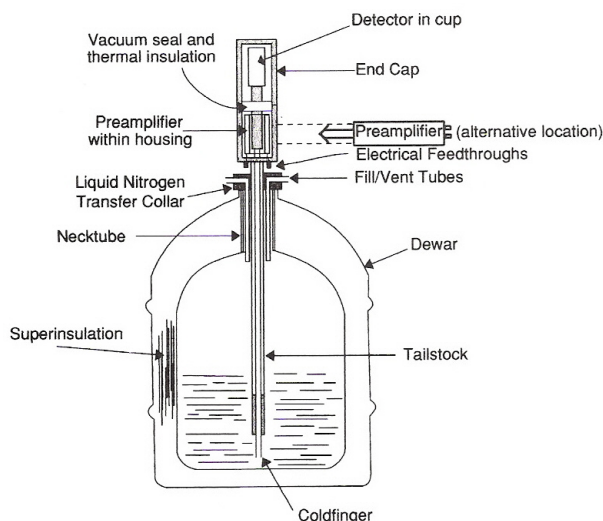
5 Gamma Spectrometry [2]

The gamma ray energy spectrum is used to identify radioactive isotopes. In the laboratory of the Radioactivity Section high purity germanium detectors are used for gamma spectrometry. Germanium is a semiconductor element which can be brought to very high purity in special zone refinings, high purity means that very few foreign atoms are present in the crystal. How can gamma rays be detected in a germanium crystal: The band gap between the valence and the conduction band in germanium amounts to 0,74 eV and the necessary energy for the production of an electron-hole pair amounts to 2,96 eV. If now a typical gamma quantum of about 1 MeV gets into the crystal, then about $3,4 \cdot 10^5$ electron-hole pairs (charge carriers) are produced. This leads to an electric current of approximately $1\mu\text{A}$. In order to measure such small currents exactly, the cutoff-current in the crystal must be smaller by several orders of magnitude. The cutoff-current depends on the density of the intrinsic charge carriers and on the number of impurities. Thus one must keep this number of charge carriers as small as possible. This is done first of all via improved cleaning methods and secondly with cooling. Cooling of the material reduces clearly the density of the intrinsic charge carriers by setting the conduction band empty. However these two measures do not lower the cutoff-current sufficiently, additionally special electrical contactings of the crystal external wall must be selected. The detectors are operated as inverse diode: As an example the entrance window of an n-type detector is highly endowed with holes (p^+) (e.g. boron) and the other side as n^- contact (e.g. lithium). The energy resolution of a germanium gamma spectrometer for a photon of 1 MeV is approximately 1.7 keV. The statistical uncertainty is proportional to the square root of the number of charge carriers. Multiplication of this number with the energy necessary to create an electron-hole pair leads to the energy resolution. This is the main reason why germanium detectors are much better for high resolution gamma spectroscopy than the NaI(Tl) scintillation detectors which needs approximately 3 keV to produce one counting event and thus the resolution is 40 times weaker. With a scintillator it would not be possible to differentiate isotopes emitting gammas withing an 60 keV energy interval.

5.1 Interaction of gamma rays with material

Gamma rays are photons of the nucleus and fullfill the relation $E = h\nu$. Photons with energies above 10 keV are called gamma rays. This is only a part of the whole electromagnetic spectrum in which visible light is contained. Visible light has energies of a few eV only and is thus more than a thousand times smaller in energy than gamma

Figure 5.1: Set up of a germanium gamma spectrometer cooled by liquid Nitrogen



rays. In atomic physics one speaks of the outermost electrons, the so called valence electrons, which can undergo optical transitions. It means that their binding energy is of a few electronvolts. Gamma rays on the other hand originate of nuclear de-excitations. Photons are spin 1 bosons and carriers of the electromagnetic interaction. They will thus interact with charged particles. In our case these are especially negatively charged electrons. There are different types of interaction of photons with electrons known as

- Photoelectric effect
- Compton scattering
- Pair production

5.1.1 Photoelectric effect

The discovery of this effect yielded the Nobel prize for Albert Einstein in 1921. The experiment of taking a metal of the alkaline series and connecting it to an electric circuit provided a small electric current if the metal was exposed to light. This fact can be explained only in considering light as particles where photons carry a quantum of energy and can transfer it in inelastic shocks. Photons of a certain energy E_γ ionize atoms by liberating one of their valence electrons. The liberated electrons achieve a certain kinetic energy E_e if E_γ is bigger than the binding energy E_b . The kinetic energy is thus $E_e = E_\gamma - E_b$. The photon loses all its energy to the electron and disappears. The atom remains in an excited state and can de-excite in different ways. One possibility is that the vacancy left by the photoelectron is filled with another electron of the same atom. In the case of gamma rays the liberated electron is in general a K-shell electron, this is the innermost shell. Filling of such a gap leads to the emission of characteristic X-rays

which are absorbed in turn until ultimately all the energy of the gamma ray is absorbed by the material. The probability that a photon will undergo photoelectric absorption can be expressed as a cross section τ . This will be a function of the atomic number Z of the absorber and the gamma ray energy E [2]

$$\tau \propto \frac{Z^n}{E_\gamma^m} \quad (5.1)$$

where n and m are within the range 3 to 5 depending upon energy. Usually the larger Z the bigger the probability to undergo photoelectric effect. It follows that ideal detector material is of high Z , given that their charge collection characteristics are satisfactory.

5.1.2 Compton scattering

This is a direct interaction of the incident gamma photon with an electron in which the photon transfers only part of its initial energy E_γ to the electron. The remainder of the original photon's energy is emitted as a new, lower energy gamma photon with an emission direction different from that of the incident gamma photon. The energy the electron obtains is

$$E_e = E_\gamma - E_{\gamma'} \quad (5.2)$$

The probability of Compton scatter decreases with increasing photon energy. Compton scattering is thought to be the principal absorption mechanism for gamma rays in the intermediate energy range 100 keV to 10 MeV. Compton scattering is relatively independent of the atomic number of the absorbing material. With θ being the scattering angle of the photon the energy can also be computed to

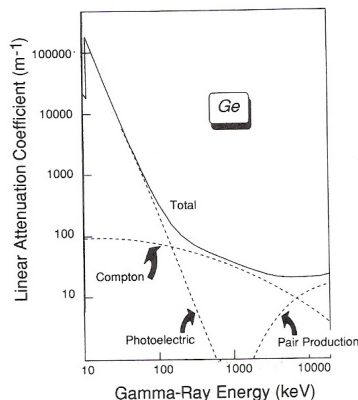
$$E_e = E_\gamma \left[1 - \frac{1}{1 + \frac{E_\gamma[1-\cos\theta]}{m_0c^2}} \right] \quad (5.3)$$

where m_0c^2 is the rest energy of the electron.

5.1.3 Pair production

As the word says something is produced out of a gamma ray. According to Einsteins formula $E = mc^2$ energy can be transformed to matter and vice versa. In pair production an electron e^- and a positron e^+ are produced. The process takes place within the Coulomb field of the nucleus. For this quantum mechanical effect the gamma-ray must carry an energy at least equivalent to the combined rest mass of the two particles making 1022 keV in all. In practice evidence of pair production is only seen when the gamma energy is rather more than 1022 keV see figure 5.2. The electron and positron pair share the excess gamma-ray energy equally, losing it to the medium as they are slowed down. When the energy of the positron is reduced to thermal energies it must meet an electron

Figure 5.2: Attenuation coefficient for Compton, pair production and photo effect. Photoelectric effect $\sim \frac{Z^5}{E^2}$, Compton scattering $\sim \frac{Z}{E}$ and pair production $\sim Z^2 \ln(E)$. For detectors of high Z there are more photoelectric effects than compton scatterings. Source [2]



of an atom and the two will annihilate releasing two 511 keV annihilation photons. This opposite process is likely to happen within 1 ns of creation. The charge collection time of detectors is 100 to 700 ns, the annihilation can thus be regarded as instantaneous with the pair production event.

5.2 Interaction with the detector

The interaction is always transfer of the gamma-ray energy to electrons or in pair production to electrons and positrons. The energy of these individual particles can range from near zero to the full energy of the gamma-ray. As already mentioned gamma-rays cover an energy range from a few keV to many MeV. Comparing this energy to the energy of 2.96 eV necessary to create an ion pair in germanium it is obvious that one gamma-ray will produce many electron-hole pairs. The expected number of ion pairs is thus

$$n = \frac{E_e}{\varepsilon} \quad (5.4)$$

where E_e is the energy of the primary electron excited by the gamma-ray and ε is the energy needed to create the ion pair. These generated secondary electrons and their associated positively charged holes must be collected in order to produce the electrical signal from the detector.

5.2.1 The large detector

Consider an infinitely large detector as drawn in figure 5.3 which is bombarded with gamma-rays of an energy above 1022 keV. Because the detector is large we can assume that every gamma-ray will have an opportunity to interact by one or other of the three main processes mentioned before. Every gamma-ray will thus deliver its total energy to the detector, nothing is lost. Many Compton scatterings and many pair production will occur until all the initial energy is transferred to the detector.

5.2.2 The small detector

This detector shall be defined so small that only one interaction can take place within it. In this case only photoelectric interactions will produce full-energy absorption and contribute to the full-energy peak. Because of the small size of the detector all Compton scattering events will produce only a single recoil electron carrying only a portion of the whole gamma energy. The scattered photon will escape from the detector as one can see in figure 5.3 and this energy will be lost to counting leading to so called single or double escape peaks. The energy absorbed by pair production events is limited to the energy excess of the electron-positron rest masses. It can be assumed that both will transfer their kinetic energy to the detector but the two annihilation gamma-rays will escape from the detector which leads to the double escape peak. Where one finds a peak 1022 keV below the full energy peak see figure 5.5.

5.2.3 The real detector

Any real detector represents a case between these two extremes (figure 5.4). There will be many Compton scatterings and pair productions leaving all the energy in the detector and thus contributing to the full-energy peak. But there will also be some Compton scattering events followed by others, each absorbing a little bit more of the initial energy, before the scattered gamma-ray escapes from the detector. Such events are referred to as multiple Compton events. For pair production there is the possibility that after annihilation only one photon escapes leading to a single escape peak 511 keV below the full energy peak.

5.3 High purity germanium crystals

Polycrystalline germanium of already high purity is further purified by zone refining. The germanium is melted using radio-frequency heating coils. Impurities will then concentrate in the liquid phase. The solid phase at the same time is left purer than the original melt. There are several zone refiner coils and each of them melts a small portion of the germanium. As the coil is slowly moved along the length of the crucible the molten

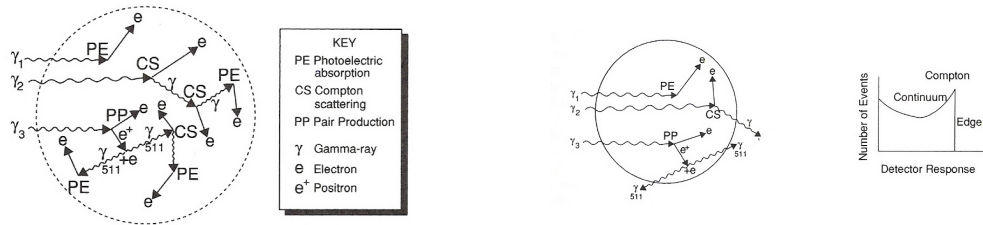


Figure 5.3: Interactions within a large detector on the left and within a small detector on the right. Source [2]

Figure 5.4: Interactions within a real detector. Something between the large and the small detector. Source [2]

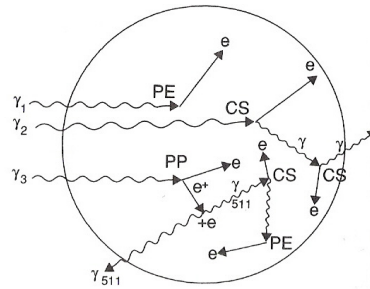
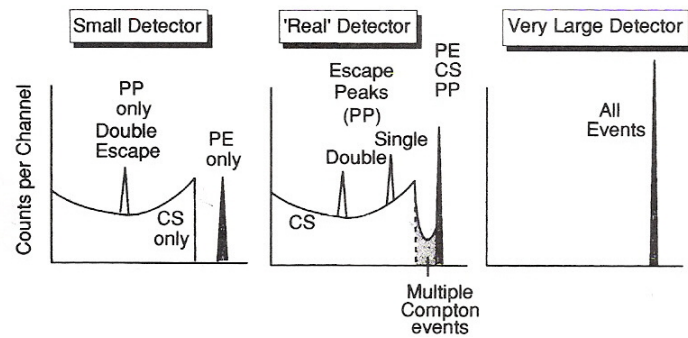


Figure 5.5: The three different approaches to detectors would lead to those three different spectra. Source [2]



zone moves with it. The germanium melts as the coil approaches and freezes as the coil moves away, leaving a higher concentration of impurities in the liquid than the solid. In this way the impurities are swept along in the molten zone to the end of the bar. Many sweeps are needed and finally the tapered end of the germanium bar contains most of the impurities and can be cut off.

5.4 Calibration of the Multi Channel Analyzer MCA

The produced current in the detector is analyzed through a large setup of electronics. First the signal is amplified then digitalized and finally gets into a multi channel analyzer where each channel represents a certain energy range. The relationship between the absorbed energy and the channel number is almost linear. Before doing precise measurements the MCA has to be calibrated. Doing this one uses standardized radioactive samples with known energies and activities of the nuclides.

5.4.1 Energy calibration

During the energy calibration primarily the emitted gamma energies are assigned to the appropriate channel numbers of the multichannel analyser. For the calibration a preparation is needed, which exhibits at least two gamma lines in the energy region which can be measured. Still it is better to use a radioactive preparation with 3-5 lines distributed over the whole measured energy range. The activity of the preparation does not play a substantial role, it should however be in the size that one gets to a reasonable counting statistics in finite time.

After taking up the spectrum a 2 point calibration is accomplished with the energetically lowest and the energetically highest photo peak in the spectrum. For an exact energy calibration however if possible all lines existing in the spectrum should be considered. For an energy calibration in the measuring range 50 keV to 2 MeV the nuclide mixture given in table 5.1 is suitable: The relation between channel number and energy is almost

Table 5.1: Mixture of 3 nuclides used for energy calibration. Source [15]

Nuclide	γ -ray Energy [keV]
²⁴¹ Am	59.54
¹³⁷ Cs	661.66
⁶⁰ Co	1173.24
⁶⁰ Co	1332.50

linear. However it is best described by a square function, whereby the square term is very small and refers to quasi linearity.

5.4.2 Peakform calibration

The peak form calibration describes the resolving power of the measuring system as a function of energy. During the peak form calibration the asymmetry of the Gauss form over the energy of the photo peaks is determined. This calibration is accomplished always together with the energy calibration by the multichannel analyser systems. The resolution of a gamma system is described by the so-called half width. The half width is those width of the photo peak in half height, one shortens it with $FWHM = \text{Full Width at Half M}^{139}\text{Ce maximum}$. This depends on the energy and increases with rising energy. σ is the standard deviation of the gaussian peak.

$$FWHM = 2.35 \cdot \sigma \quad (5.5)$$

A photon of the energy $E_\gamma = h \cdot \nu$ should provide a discrete line in the spectrum but according to the finite lifetimes of the energy states and Heisenberg's uncertainty relation $\Delta E \sim \Delta t$ there is an uncertainty in energy leading to a broadening of the peak. The detector type contributes as well to the peak width, the easier it is to create electron-hole pairs the more such pairs will be created for a certain photon energy leading to more counts n and to better statistics. In general the peak width is a function of energy and can be described by the following empirical formula:

$$w = a + b \cdot E_\gamma \quad (5.6)$$

where a and b are empirical constants. Such a linear relationship is adequate over a large energy range. In practice the resolution for the 1173 keV ^{60}Co line is 2 keV whilst for a NaI(Tl) scintillator it would be 70 keV.

5.4.3 Efficiency calibration

The efficiency of the germanium crystal depends on its design, on the energy of the photons and on the used sample geometry. During the efficiency calibration the efficiency of the measuring system is determined over the adjusted energy region. For each detector and for each sample geometry which is used its own calibration is to be accomplished. Since the samples coming to the measurement can be very different, the calibration is usually accomplished with a water-similar standard, i.e. a mixture from different radionuclides embedded in a material of the density 1 kg/dm^3 and the same elemental composition. During the measurement of gamma spectra the following problems arise in particular:

- Absorption in the sample
- True coincidence summing

5.4.4 Absorption in the sample

The photons emitted by the sample material are weakened in interactions with the sample material. The intensity of the radiation follows the Lambert-Beer law

$$I(x) = I_0 e^{-\mu x} \quad (5.7)$$

where μ is the mass absorption coefficient and x the thickness of the sample. This absorption depends on the one hand on the cross-sections of the different elements contained in the sample as well as on the density of the material. During the measurement thereby counting losses arise. If now the sample and the standard used for the calibration consist of strongly different materials, this effect has particularly strong effect on the measurement. We use the simulator routine "GESPECOR" (Germanium SPECTroscopy CORrection developed by Prof. Sima, University of Bukarest), which computes this weakening depending upon material and sample geometry by Monte Carlo simulations.

5.4.5 True coincidence summing

If radionuclides are used, which exhibit transitions which lead to an emission of two or several gamma quanta in direct consequence in their decay patterns, the emitted gamma quanta can be counted partially only together. This leads to counting losses in the photo peaks of the individual lines and to counting surplus at the energy, which develops from addition of the energy of the photons arrived at the same time. This so-called coincidence summation does not only arise with cascade transitions, but can also occur with gamma- and x-rays coming from different elements at the same time. An example is given for ^{134}Cs in figure 5.6. The probability that two photons arrive at the same time into the detector and be counted only together thus, rises with larger solid angle and activity. If the solid angle is very small, it is very improbable that two photons arrive at the same time into the detector. Since in our case the samples exhibit however only a very small activity, we must bring them as near as possible to the detector. Thus the solid angle and the probability for coincidence summation rise. This problem can be corrected again with the software "GESPECOR".

5.4.6 Suitable nuclide mixtures

For the efficiency calibration one needs nuclide mixtures, which exhibit a multiplicity of gamma lines. Such certified mixtures are manufactured by internationally recognized institutes. According to the energy range of 50-2000 keV standard mixtures are offered. At low energies up to approximately 200 keV the individual lines should be relatively close, this because at this energy the efficiency of the detector strongly changes. For higher energies fewer lines are sufficient, but distributed well over the whole remaining energy region. A typical mixture is given in table 5.2. Positive at the given mixture

Figure 5.6: Measurement of ^{134}Cs with two strong lines at 600 and 800 keV and their summation peak at 1400 keV. Source [20]

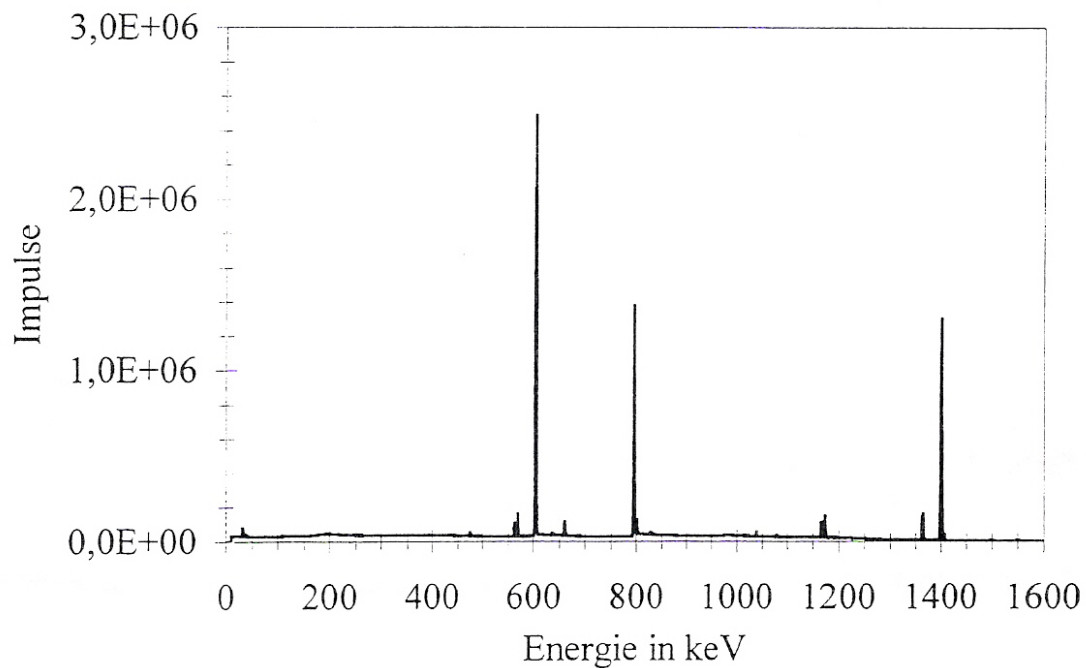


Table 5.2: Standard nuclide mixture for the range 50keV-2MeV. Source [15]

Nuclide	$T_{1/2}$ [d]	Energy [keV]	Intensity [%]
^{133}Ba	3842	79.62	2.61
		81	34
		276.39	7.1
		302.85	18.33
		356.01	62.3
		383.85	8.92
^{57}Co	271.84	122.06	85.59
		136.47	10.58
^{139}Ce	137.65	165.85	80
^{85}Sr	64.85	514.01	98.4
^{137}Cs	11050	661.66	85
^{54}Mn	312.5	834.84	99.98
^{65}Zn	243.9	1155.55	50.4
^{88}Y	106.66	898.04	94.6
		1836.06	99.24

in table 5.2 is its good distribution of the photo peaks and the long radioactive half-life of the elements, so that the calibrations can be accomplished also during a longer period with the same standard. A disadvantage forms the element ^{88}Y and above all the element ^{133}Ba , which exhibits 6 lines, thus develops many losses by cascade effects. One can replace the barium, frequently one is however forced to use radionuclides with short half-lives, which limits the use of the standard temporally. Another isotope currently used is ^{60}Co with its two lines at 1173 keV and 1332 keV. The problem here is also the probability for true coincidence summing falsifying results for the natural ^{40}K lying in the same range with its 1460 keV line. The activities of ^{40}K tend to be overestimated without a true coincidence summing correction.

5.4.7 Execution of the calibration

With the calibration sample available in the appropriate sample geometry a gamma spectrum is taken up. The measuring time should be in the order of magnitude that at the conclusion all photo peaks coming to the evaluation have a net area of at least 2000 counts, so that the statistic uncertainty is as small as possible. The energy dependent efficiency $\eta(E)$ computes itself as follows.

$$\eta(E) = \frac{\text{Counts}}{A \cdot p(E) \cdot t} \quad (5.8)$$

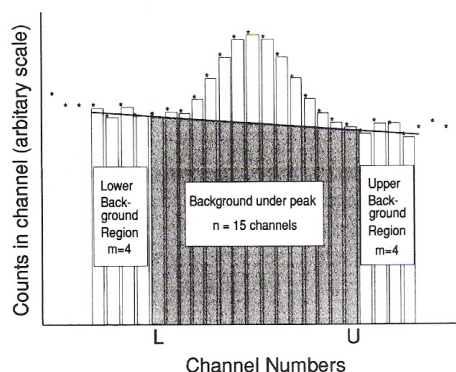
Where A is the activity of the radionuclide emitting at energy E and $p(E)$ is the emission probability of a photon of that energy and t the measuring time.

5.5 Peak calculations

As explained in the calibration section a background file is measured which is afterwards subtracted of the radioactive sample file. Natural radioactivity such as ^{214}Pb , ^{212}Pb , ^{212}Bi and ^{40}K and will also be present in the background file and provide energy peaks. If we do measure now natural radioactivity in our sampled filters the peaks already present in the background must be subtracted from the whole peak as well as the continuous background below the peak. It means that in the big peak a small background peak is integrated and the background continuum below the peak must be cut off see figure 5.7. The analyzing program Inter Winner provides three different values for peak calculations:

1. Gross counts(G)
2. Net counts(N)
3. Net-Background(n)

Figure 5.7: The shaded background is subtracted from the net peak area. Source [2]



The gross count rate G is the number of counts in the whole big peak. The net count rate N is the peak above the background continuum and the effective counts of the sample are given by Net-Background n , which subtracts the natural peak coming from background.

In statistics the uncertainty is usually given by the square root of the respective number. We measure a net countrate N and the statistical uncertainty would therefore be \sqrt{N} . The number leading to the radioactivity of a sample is n : Net minus Background. To evaluate its uncertainty one uses the following formula:

$$\sigma_n = \sqrt{n + 2(G - n)} \quad (5.9)$$

Usually one uses a 2σ confidence interval, meaning that the real value is contained in it to a probability of 95%. The relative uncertainty in percent of the Net-Background counts resp. total statistical relative uncertainty is thus:

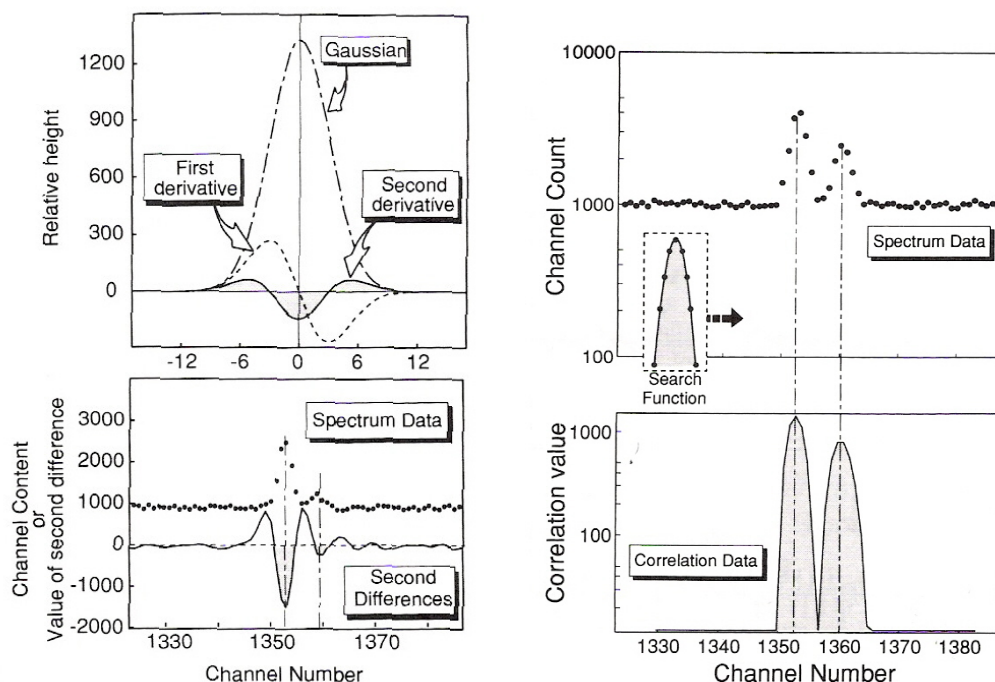
$$\sigma_{\text{Stat}} = 2 \cdot \frac{\sqrt{n + 2(G - n)}}{n} \cdot 100 \quad (5.10)$$

5.5.1 Peak search

A computer software is responsible for the peak search. There are different mathematical procedures. The method of derivative peak searches and peak searches using correlation methods shall be explained briefly (See figure 5.8).

Derivative peak search This method uses first and second derivative of a Gaussian curve calculated for the data. Both derivatives have features which can be used to detect the presence of peaks. As an example the first derivative changes its sign as it

Figure 5.8: The figure on the left belongs to derivative peak search. The figure on the right represents the correlation method. Source [2]



crosses the peak centroid and the second reaches a minimum. Gamma-ray peaks are of course not Gaussians but histograms which approximate a Gaussian curve. Thus one cannot calculate a differential as such but must use the differences between channels as an approximation to the gradient.

Correlation methods This method is based upon cross-correlation. A Gaussian search function is scanned across the spectrum multiplying each spectrum count. The sum of these products is then a point on the correlation spectrum. After subtracting the underlying continuum, any channels which are greater than zero represent channels within a peak.

5.6 Software

5.6.1 InterWinnerTM analyzing program

For the evaluation of the radiation measured by the detector we use the gamma and alpha spectroscopy software InterWinnerTM of Ortec. Before starting the measurement,

one can enter various parameters to the program which would be:

- Store the spectrum to a certain name
- Input of the gate time at expiration of which the measurement is stopped or input of a special peak net area after which the program stops the recording, as soon as this surface is reached
- Selection of the isotope library
- Selection of the background- and the efficiency curve

InterWinner permits to evaluate the measured data already during the acquisition time, without disturbing the further counting events. The evaluation of a gamma spectrum requires several steps, which the program is to settle all together:

- Peak search
- Subtract the background below the peak
- Calculate position and amplitude of the peaks
- Determination of the nuclide-specific activity using the isotope library and the efficiency curve
- Decay correction of the activities for the decay during the measurement
- Averaging the activity of nuclides with several lines
- Consideration of uncertainty

5.6.2 Decay correction

In accordance to the law of radioactive decay 2.2 always the same portion of radioactive elements decay in same time periods, independently of the age of the sample. This leads to the fact that the so-called half-life is a very common size. It is the time, after which the number of initial nuclides decreased by half.

$$T_{1/2} = \tau \ln 2 = \frac{\ln 2}{\lambda} = \frac{0.6931}{\lambda} \quad (5.11)$$

Now if the acquisition time is short compared to the life span of the contained radioactive nuclides, then one can simply divide the peak net area F by the effective acquisition time (live time t_l) in order to receive the net counting rate. The activity of a certain element can be computed directly with consideration of the efficiency of the detector ϵ and the γ -emission probability.

$$A = \frac{F}{\gamma_i \epsilon_i t_l} \quad (5.12)$$

However if the live time is longer, then one must consider the radioactive decay during this time. The activity becomes a function of the time according to formula 5.13

$$A(t) = \lambda N(t) = \lambda N_0 e^{-\lambda \cdot t} \quad (5.13)$$

And the expected peak area calculates to

$$F_i = \int_0^{t_r} A(t) \gamma_i \epsilon_i \frac{t_l}{t_r} dt = \gamma_i \epsilon_i \frac{t_l}{t_r} \lambda N_0 \int_0^{t_r} e^{-\lambda t} dt = \gamma_i \epsilon_i \frac{t_l}{t_r} \lambda N_0 \frac{1 - e^{-\lambda t_r}}{\lambda} \quad (5.14)$$

If one substitutes λN_0 with the activity A and solves for it one gets the activity for a nuclide i

$$A_i = \frac{F_i}{\gamma_i \epsilon_i t_l} \cdot \frac{\lambda t_r}{1 - e^{-\lambda t_r}} \quad (5.15)$$

If the real acquisition time t_r is much smaller than the respective half-life ($t_r \ll 1/\lambda$) formula 5.15 reduces to 5.12.

5.6.3 Decay correction during sampling time

In our case air filters are sampled during two weeks or longer this leads to the fact that one has to consider already a decrease in activity during this time. If one assumes constant activity deposit per unit of time a ($[a] = [s^{-2}]$), then the total activity after run off time T can be determined by integration.

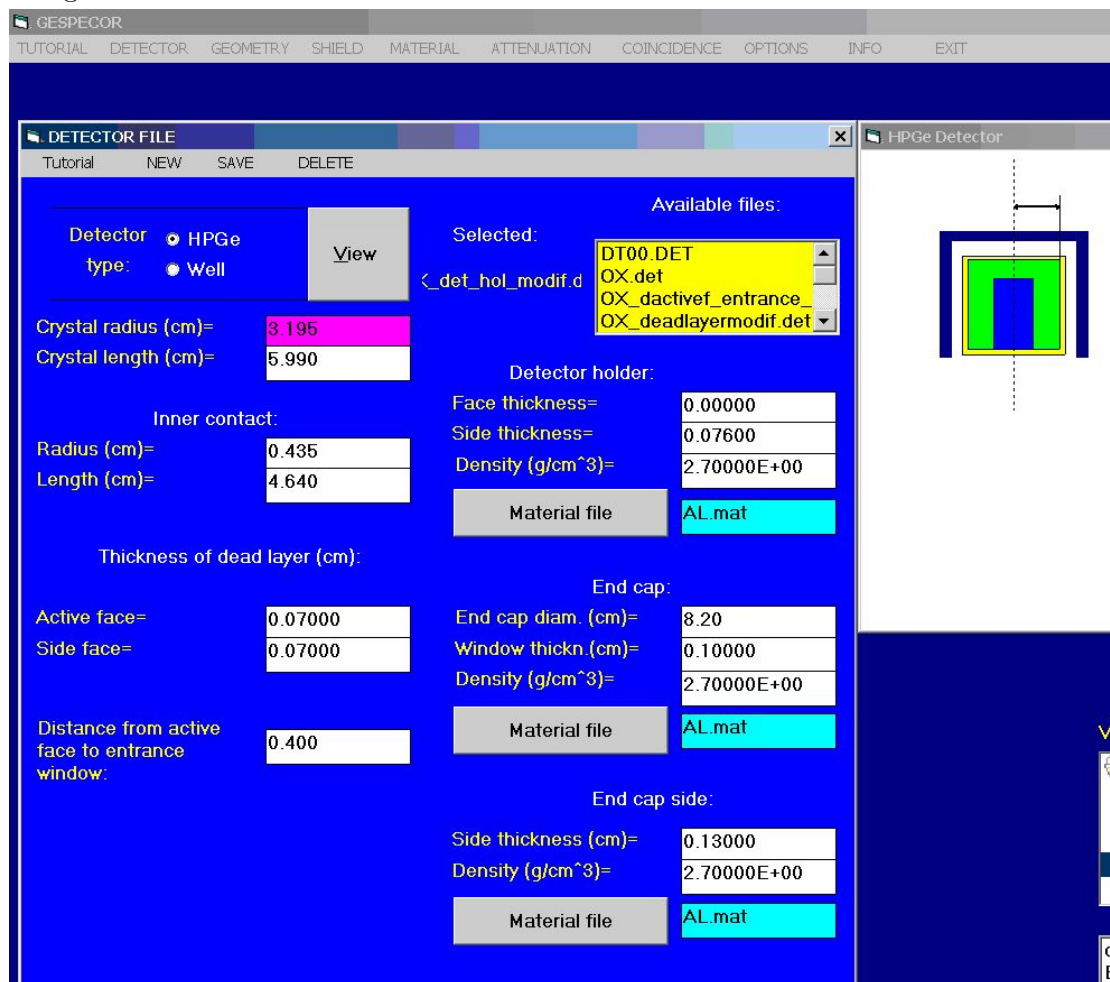
$$A = \int_0^T a e^{-\lambda(T-t)} dt = a e^{-\lambda T} \int_0^T e^{\lambda t} dt = a e^{-\lambda T} \frac{e^{\lambda T} - 1}{\lambda} = a \frac{1 - e^{-\lambda T}}{\lambda} \quad (5.16)$$

In the limit of large half-lives compared to the sampling time T formula 5.16 reduces to $A = aT$

5.7 GESPECOR

Gespecor is the abbreviation of GERmanium SPEctrometry CORrection developed by Prof. Sima from the University of Bukarest in collaboration with PTB Braunschweig [20]. It is a program which uses Monte Carlo simulations to supply correction factors for the gamma spectroscopy. Monte Carlo methods [13] are a widely used class of computational algorithms for simulating the behavior of various physical and mathematical systems. They are distinguished from other simulation methods (such as molecular dynamics) by being stochastic, that is nondeterministic in some manner - usually by using random numbers (or more often pseudo-random numbers) - as opposed to deterministic algorithms. Because of the repetition of algorithms and the large number of calculations involved, Monte Carlo is a method suited to calculation using a computer, utilizing many techniques of computer simulation. Important are corrections concerning self-absorption in the sample and nuclide-specific coincidence summations. So that the program accomplishes good computations, first a whole row of parameters must be entered to it. Those are first of all various parameters of the detector: The shown window 5.9 serves for the selection of the type of detector (borehole or coaxial detector) as well as the definition of the dimensions of the germanium crystal, the holder, the end cap and also for the

Figure 5.9: The known dimensions of the detector must be entered in this window.



selection of the materials building the detector. It is to be said that only data of one detector are presently known to us, therefore only those measurements, which were accomplished with this detector are meaningfully corrected. Next one must enter geometry and composition of the sample container as exactly as possible, in addition internal and outside radius as well as internal and outside height of the cylindric container must be determined. Very important is also the used material. The program possesses a data base in which various materials are given from which one can select. (see figure 5.10) Since a correction factor for the self-absorption of the sample is computed (figure 5.11), the program needs also exact data concerning chemical composition and density of the sample. On the basis of tabulated activation cross-sections the program is able to compute the absorption of photons of different energies in the sample. The program must know the sample geometry and composition of the cylinder, in which the sample is in it. These data are indicated in the window "Geometry file" see 5.10. On the basis of the

Figure 5.10: Everything about the sample geometry is entered here.

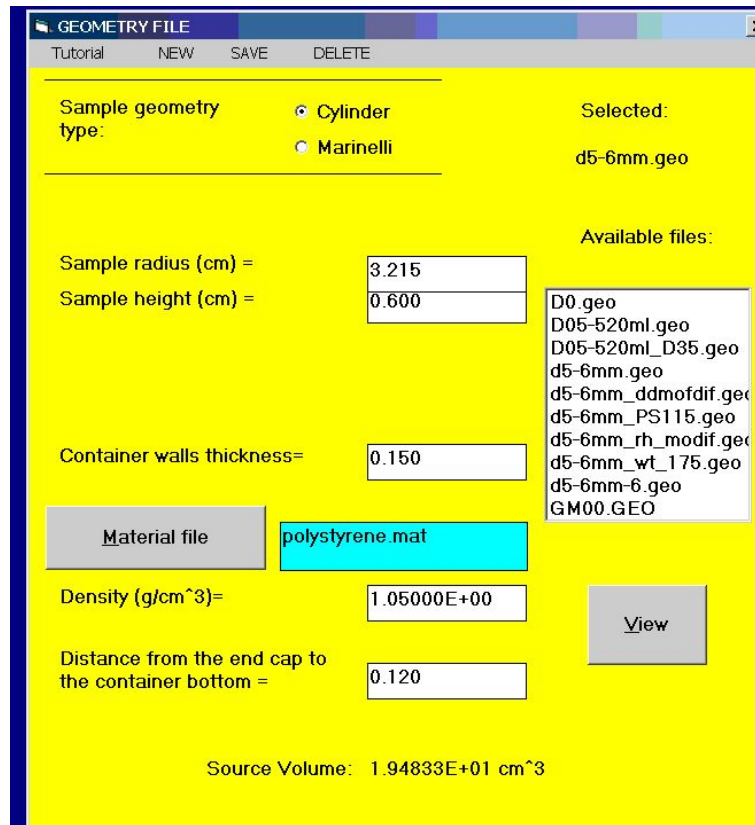


Figure 5.11: Self attenuation correction factors are calculated here.

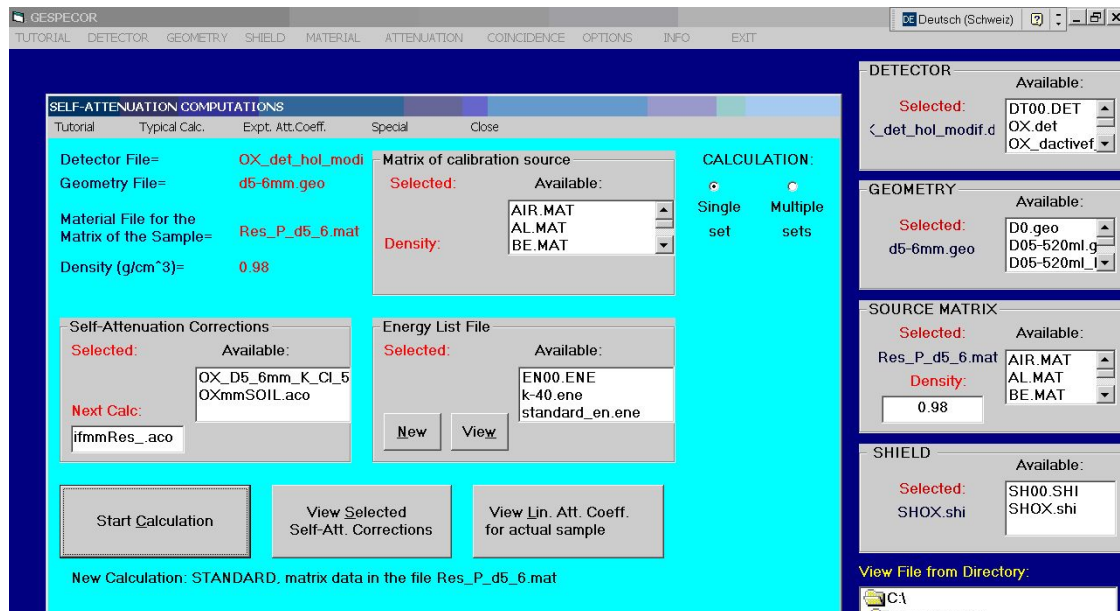


Table 5.3: GESPECOR correction factors calculated for our sample geometry and with the density of 4 sampled glass fibre filters of about 0.5 kg/dm^3 in contrast to the calibration standard of 0.98 kg/dm^3 . Because of the thinner sample the activities are overestimated and must therefore be divided by those factors greater than 1. F_{CA} is the correction for absorption in the sample which decreases with increasing energy and F_{TCS} is the correction for true coincidence summing being quite important for ^{214}Bi and ^{208}Tl which have many gamma transitions. The mono-gamma emitters remain uncorrected for TCS.

Isotope	Energy [keV]	F_{CA}	F_{TCS}	$F_{CA} \cdot F_{TCS}$
^{210}Pb	46.54	1.05608	1	1.05608
^{212}Pb	238.63	1.02827	0.99982	1.02808
^{214}Pb	295.22	1.02622	1.00160	1.02786
^7Be	477.6	1.02176	1	1.02176
^{208}Tl	583.19	1.02000	0.83488	0.85158
^{214}Bi	609.31	1.01962	0.86375	0.88070
^{137}Cs	661.66	1.01892	1	1.01892
^{212}Bi	727.33	1.01814	0.95219	0.96946
^{40}K	1460.82	1.01290	1	1.01290

entered data Gespecor computes correction factors for any energy in the spectrum, which considers self-absorption in the sample. One can indicate for which energies one would like to have computed those factors because absorption depends on energy. Gespecor calculates only true coincidence correction factors F_{TCS} for elements with more than one line. The elements emitting one single gamma thus remain uncorrected and have 1 as factor as indicated in table 5.3. For elements with several lines usually the line with the highest emission probability is taken in order to calculate the activity.

5.8 Uncertainty budget

Measurement uncertainty takes account of errors involved in physical measurement. Any physical measurement comprises two parts: an estimate of the true value of the measurement and the uncertainty of this estimate. The estimate of the physical quantity is always erroneous. It can thus only be said by adding an uncertainty in which environment of the estimate the true value is.

In our measurement many sources of uncertainty contribute to the final result. The occurring sources were estimated by the heads of the Radioactivity Section Dr. Sybille Estier and Prof. Dr. Hansruedi Völkle to be as follows:

- Uncertainty of the sampled volume $\sigma_Q=2.5\%$
- Uncertainty of calibration and calibration standard $\sigma_C=5\%$

- Uncertainty of decay correction $\sigma_D=1\%$
- Uncertainty of the nuclide library $\sigma_N=1\%$
- Uncertainty of the software for peak calculations $\sigma_S=2\%$
- Statistical uncertainty $\sigma_{Stat}=\text{see formula 5.10}$

All these individual relative uncertainties contribute to the final result, which in our case is an activity per volume air. One gets the final uncertainty by taking the square root of the sum of the squares of relative errors.

$$\sigma_{Tot} = \sqrt{\sigma_Q^2 + \sigma_C^2 + \sigma_D^2 + \sigma_N^2 + \sigma_S^2 + \sigma_{Stat}^2} \quad (5.17)$$

6 Digital DHA-80

The DIGITEL DHA-80 by Digital Elektronik AG is a system for the collection of dust and aerosol particles to the later evaluation and analysis. The air flow amounts to 6 - 60 $\frac{m^3}{h}$. One calls such systems High volume air sampler HVS. The Radioactivity Section runs 5 different and older high volume samplers in Switzerland with an air flow of up to 600-700 $\frac{m^3}{h}$

The aerosols of the sampled air are separated on round glass fibre filters of 150 mm in diameter. The effective area of the filter amounts to 140 mm. The choice of the filter material and the filter structure depends on the investigation goal. The DHA-80 has a magazine with 15 filters, which are clamped in filter holders. These are exchanged at the pre-programmed time automatically into the sampling position. The desired air volume is preselected at a rotameter. This value is to calibrate at the beginning of the measuring campaign with a secondary standard. During sampling the power of the pump is dynamically changed in such a way that the flow-through volume is kept constant with a long term stability. This applies in particular regarding change of flow resistance on the filter as well as in change of pressure and temperature of the ambient air. An inserted microprocessor steers the filter change time-exactly and collects all relevant data and events. The amount of air led over the filter is defined therefore with large accuracy. Figure 6.2 illustrates the mode of operation. The air is sampled via a sampling probe (1), using a sampling tube, vertically from the top to the bottom through the filter (3) placed in the flowing chamber (2). The velocity of the sampled air amounts to 0.5 m/s at a 500 l/min flow rate. After the filter, the transported air quantity is measured using a flow meter with a floater (5). Its double photo-sensor (5a) optically senses the floater position. In connection with the control electronics (5b, 5c), the capacity of the pump (6) is adapted to the rpm control, so that the air quantity keeps the set-point value. Air pressure and temperature are measured upstream the flow meter and continuously averaged by the controller. A real-time protocol states sampling volumes yielding from the sampling time and controlled volume flow as the core information. The air is released from the instrument with reduced noise through a noise baffle (7).

The high volume sampler was conceived for a network and can be steered either via an internet connection or directly at the apparatus via a key field. Filter changes and control of the pump are steered via a hyper text transfer protocol window (figure 6.3) whilst changes of steering elements such as work time, pause time, flow-through-volume needed for the volume calculations etc. must be entered in the steering document "dmcu.ini" and transferred via a file transfer protocol ftp. All the modifications can thus be accomplished remotely except two: Altering the height of the light barrier which steers directly the



Figure 6.1: The Digital DHA-80 in Fribourg. Inside top on the left the keyboard, below the filter reservoir and on the lower left the floating element

power of the pump and therefore the flow-through-volume must be made directly at the machine as well as taking out the sampled filters and refill the filter reservoir.

6.1 Air Volume

The power of the engine is adapted in such a way that the floating element of the rotameter stays always on the same height. This regulation provides a constant air flow through the filter and guarantees a well calculated value for the volume.

The floating element is in a glass tube on which a millimeter scale is etched in. The respective hover height corresponds to a certain volume in standard conditions of 288 K and 1013 hPa, which had to be determined with the measuring of the glass tube. On this basis the flowing air volume can also be computed in other conditions. In addition one sets the light barrier of the floated element to a certain height, switches the turbine on and reads off the height of the floated element. This height corresponds to a certain air volume, which is to be found tabulated in the user manual of the DHA-80 at standard conditions. In order to compute the promoted air volume at current conditions one makes use of the following formula:

$$Q_{loc} = Q_{Skala-innen} \sqrt{\frac{p_{ref} T_{mM}}{p_{mM} T_{ref}}} \quad (6.1)$$

Figure 6.2: Conception of the Digital DHA-80. 1. Pre-Separator; 2. Separator chamber; 3. Current filter; 3a. Filter stock; 3b. Used filter; 4. Microprocessor control; 5. Flow meter; 5a. Flow sensor; 5b. Flow control; 5c. Frequency converter; 6. Blower; 7. Noise damper; 8. Pressure and temperature unit; 9. Printer interface; 10. RS-232C interface; 12. Wind data interface

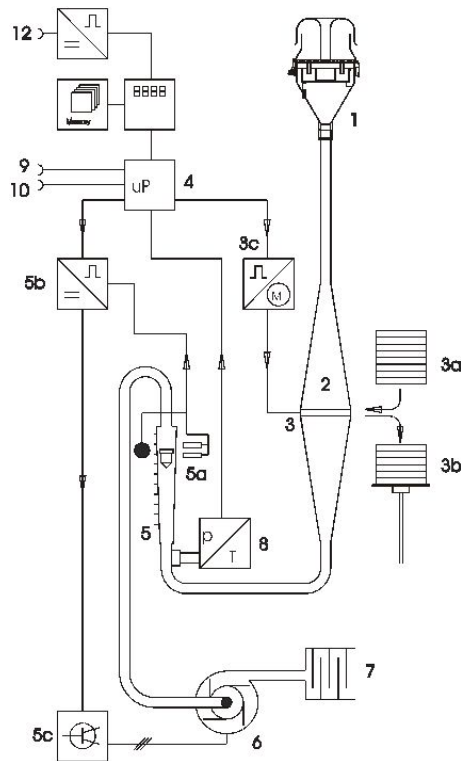


Figure 6.3: Through this interface one can start or stop the sampler and generate filter changes.

DIGITEL HTTP - Server - Microsoft Internet Explorer

Adresse http://162.23.70.50/btn_remote_on_click

DIGITEL DHA-80

Gerätekenneichen : 001-DIGITEL

letzte Abfrage : Di 21.02.06 11:22:13

Status	Fernsteuerung aus	Work	Wait	Pause	Filterwechsel
--------	-------------------	------	------	-------	---------------

Programm - Status: Work ext. 5470 min.
Fernsteuerung aktiv

Q_{loc} = Airflow at the separator at current conditions

$Q_{Skala-innen}$ = Airflow at the separator at norm conditions

p_{ref} = Norm pressure = 1013hPa

p_{mM} = Average pressure at the separator

T_{ref} = Norm temperature = 273K

T_{mM} = Average temperature at the separator

This calculation has to be accomplished each time one shifts the light barrier in order to change the flowthrough. As soon as the light is barrier on the new position, one waits about 10 min and takes thereafter the average values for pressure and temperature p_{mM} and T_{mM} . With the scale value of the floating element on the height of the glass tube one can afterwards determine the momentarily promoted air volume per minute by use of formula 6.1.

This value must be entered to the microprocessor, so that it can compute the volume promoted during the whole sampling time. There are two possibilities: One can enter the value directly at the apparatus through the keypad or adapt the value in the line "flow through to HVS" in the steering document dmcu.ini and transfer it via ftp (File Transfer Protocol) to the microprocessor.

The microprocessor computes three different volumes, for which the short designations V_N , V_M and V_A are used. V_N is the volume, which would have been promoted with given float position in the case of standard conditions. V_M is the volume, which would have been promoted considering the average values of pressure and temperature at the measuring tube during the collecting time. V_A finally is the real volume which was promoted during the collecting time. This value refers to the medium air pressure in the engine before and after sampling and the middle air temperature at the measuring tube -3K, since it is accepted that the air warms up around 3 K inside the machine. The equipment has only one thermometer inside. The outside temperature can be determined therefore only indirectly over the acceptance of a heating up of 3K. This value is not correct at cold temperatures and approaches rather 5K. This is not a problem, since this acceptance can be replaced for the computation of V_A .

$$V_M = Q_{Skala-innen} \sqrt{\frac{p_{ref} T_{mM}}{T_{ref} p_{mM}}} t_s \quad (6.2)$$

$$V_N = Q_{Skala-innen} \frac{T_{ref}}{p_{ref}} \sqrt{\frac{p_{ref} T_{mM}}{T_{ref} p_{mM}}} t_s \quad (6.3)$$

$$V_A = Q_{Skala-innen} \frac{T_A}{p_A} \sqrt{\frac{p_{ref} T_{mM}}{T_{ref} p_{mM}}} t_s \quad (6.4)$$

T_A = temperature at the air entrance

p_A = pressure at the air entrance

t_s = sampling time of the filter

The standard volume V_N and the middle promoted volume V_M would correspond themselves if during the collecting time standard conditions would have prevailed. If the temperatures and pressures are however different from standard conditions, then V_M and V_N are different, since after the ideal gas law the volume is a function of pressure and temperature.

7 Measurements

7.1 Goals

The goal of the campaign was to better understand and test the new high volume air sampling instrument Digital DHA-80 HVS-2, in order to place it in the High Altitude Research Station Jungfrauoch at 3454 m asl in the near future. The second one would be at Rochers-de-Naye at 2042 m asl above Montreux. Both locations are exposed to air mass transport from far away and can serve as good early warning monitoring stations for radioactivity. Jungfrauoch is one of 20 stations worldwide contributing to the GAW Program (Global Atmosphere Watch) of the World Meteorological Organization WMO. The collected data from other pollution and greenhouse gas parameters do also contain measurements about radioactivity in the air. Our goal is to participate in this program with our results.

Monthly measurement was aimed since December 2005. In the beginning of 2006 some software problems occurred and all the data collected before January 6th had been overwritten and erased in the data file. The sampler had to be switched off and the January measurement was shortened.

Expecting the new software version, the moment to move the instrument to Jungfrauoch had to be postponed. In the meantime the second Digital HVS-2 was installed and we decided to shorten the sampling periods and test different filtering materials, since we had both instruments in Fribourg. The sampling periods were 7-17 days depending on the availability of two detectors in the laboratory. The different filter types were always compared to the Ederol Glass Fibre filter MG 227/1/60 which had been recommended by Digital Elektronik AG and has a 99.9% efficiency at 0.3 μm . In a second phase measurements from Fribourg and Jungfrauoch are to be compared with a strong look on the naturally occurring radionuclides in air.

7.2 Procedure

The sampled filters are removed of the samplers at the end of the series of measurements folded and pressed into a cylindrical form in a hydraulic press specially developed for this measuring purpose. The press exerts a pressure of up to 15 t and forms the filters to a tablette of 6.3 cm in diameter and maximally 6 mm height depending on the amount of filters, usually four. Thus, the same geometry can be used for all measurements. The

sample geometry must be determined once and can thereafter be used as a standard for all measurements. The pressed filters are put into a cylindrical plastic container. This measuring form is put afterwards directly on the germanium detector inside the shielding see figure, 7.1. Thereby a transparent foil is put on the detector surface, in order to prevent radioactive contamination of the detector.

The gamma measuring period is approximately 2 days or 160'000 seconds. The reason for this long measuring time is the small activity of the sample. The detector does not receive more than 10 counts per second, on average. A larger measuring period improves the counting statistics and the relative error becomes smaller, which is proportional to the square root of the counts. The result of the measurement is a gamma-ray energy spectrum, where the different energy peaks can be attributed to radioactive isotopes, see figure 7.2. The determined peak net areas together with the sampled volume according to equations 2.37, 2.42 and 2.43 represent the total activity concentration of the gamma emitting radionuclides in air.

Figure 7.1: The high purity germanium gamma spectrometer OX in the laboratory Fribourg. Below the Dewar filled with liquid nitrogen ($T=-195.8^{\circ}\text{C}$). The pressed filter tablette on the detector is in a plastic box and is put inside the lead shielding for the measurement.



7.3 Sampling in Fribourg

The Digital HVS was placed on the roof of the physics department approximately 10 m above street level. The location is Chemin du Musée 3 inside the town of Fribourg. Fribourg-Marly traffic is near. Therefore fine dust concentrations is of importance especially in winter when black carbon of chimneys contribute. The filter sampling times varied between 5-22 days. In general 4 glass fibre filters of the type Ederol were sampled in those periods. As the gamma-ray detectors are in the same building five floors below, the measurement could start quickly usually within 8 minutes after the last filter change in order to achieve precise data for the short lived Radon daughter nuclides. By curiosity, the filters were weighed after the sampling time to get an idea of fine dust concentrations. Afterwards, the filters were pressed for 4-5 minutes for a suitable sample geometry and put on the detector in a plastic cylinder. The measuring time was 160 000 s as used for other measurements of the SUER. In more than 90% of all measurements the detector OX (Ortec X) was used. It is the newest one and also the most sensitive, particularly at low energies. The crystal is bigger than those of the other detectors. This leads to better counting statistics but also to a larger probability of true coincidence summing. A background file was measured on this detector with 4 unsampled Ederol filters in order to subtract especially the radiation of ^{40}K already contained in the glass fibre filter material. For some measurements the ^{40}K activity already contained in the glass fibres was more than 3 times the sampled activity of ^{40}K in the air.

7.3.1 Results

The measured isotopes are listed in table 7.1 and drawn in figure 7.3. All of those isotopes, except ^{137}Cs detected only five times, are of natural origins. Special attention is put on the natural ^7Be , ^{210}Pb , ^{212}Pb and ^{214}Pb , the first is produced by cosmic rays and the others are Radon decay products. As one can see on figure 7.3 ^7Be and ^{210}Pb correlate for the whole sampling period during this Master Thesis from December 2005 to August 2006 and reach maximum values in July. The whole month of July was characterized by stable and hot weather conditions. There were almost no low pressures and it resulted that the month of July was the warmest since the beginning of the temperature recordings in the 19th century in Switzerland. As mentioned in 4.1.2, convection in summer leads to down streaming air bringing more ^7Be downwards than in the colder seasons. The concentrations decrease in August due to frequent precipitations. The short lived ^{214}Pb and ^{212}Pb were calculated according to equations 2.37 and 2.42 and show very good correlation. This is as expected, because one must assume that they are evenly produced in earth's crust and the same convection and weather mechanisms bring them on the roof where the air sampler was positioned. Their concentrations are different: The activity of ^{214}Pb , part of the uranium decay series, is in the order of magnitude of a few Bq/m^3 and is therefore about 2 orders of magnitude higher than the ^{212}Pb activity, part of the thorium ^{232}Th daughter nuclides. This is mainly due to the much shorter half-life of ^{220}Rn ($T_{1/2}=53\text{s}$), which cannot always reach the atmosphere

and ^{212}Pb and ^{212}Bi remain and decay in the soil. Even clearer than for the longer lived ^7Be and ^{210}Pb is the correlation to precipitation. The activity decreases 4-5 times when it was raining the day before or even the day of measuring the sample (see figure 7.4).

Moreover ^{137}Cs and ^{40}K were measured. The artificial fission product ^{137}Cs coming especially from resuspension of Chernobyl-fallout was detected only 5 times and had its maximum value in the beginning of May attaining $4.8 \mu\text{Bq}/\text{m}^3$. The highest value five days after the Chernobyl accident on April 26th 1986 was approximately $500 \text{ mBq}/\text{m}^3$ [21] and therefore 5 orders of magnitude above current values but decreased exponentially the following days in May 1986. ^{40}K was difficult to detect, due to the huge half-life the activity for a given amount is small and second the glass fibre filters contain already a certain amount of potassium. This increased background makes the counting statistics and ^{40}K data poorer. The maximum value of ^{40}K was detected in July and reached $9.5 \cdot 10^2 \mu\text{Bq}/\text{m}^3$. In July, the soil was very dry and particulate ^{40}K could easily be suspended. The cosmogenic ^{22}Na was detected only once. The activity is too small to be detected regularly with our sampling settings. The five first generation HVS-1 stations, which collect 7-10 times the volume we collect with Digitel, exceed more often the detection limit.

7.4 Sampling at Jungfraujoch

The High Altitude Research Station Jungfraujoch welcomes scientists since 75 years already. At 3454 m asl the station is above most urban dust particles and makes this site extremely attractive for many scientific purposes. The SUER is present at "Top of Europe" since 1959 when a first automatic aerosol sampling station measuring beta activity was installed. The goal was and still is to better detect radioactive air masses coming from atmospheric nuclear weapon tests or other nuclear incidents. Today's studies at Jungfraujoch are focussed on climate change, greenhouse gases, atmospheric composition and aerosol research.

One of the high volume samplers was brought to the research station by train and installed on the 10th of May 2006 and sampling started immediately. Filter changes were programmed to be twice a week, needing four filters for two weeks. The last filter change before sending to the lab takes always place on tuesday evening. The house keeper of the research station sends the 4 filters individually packed wednesdays to the laboratory in Fribourg and the filters are measured usually on fridays. The sample geometry is exactly the same as used for the Fribourg filters, the filters are also the same. The flow rate was set in the beginning to be approximately 775 l/min on normal conditions ($T=288 \text{ K}$, $p=1013 \text{ hPa}$) making slightly more than 1000 l/min on actual conditions at 3454 m asl at a pressure of about 650 hPa.

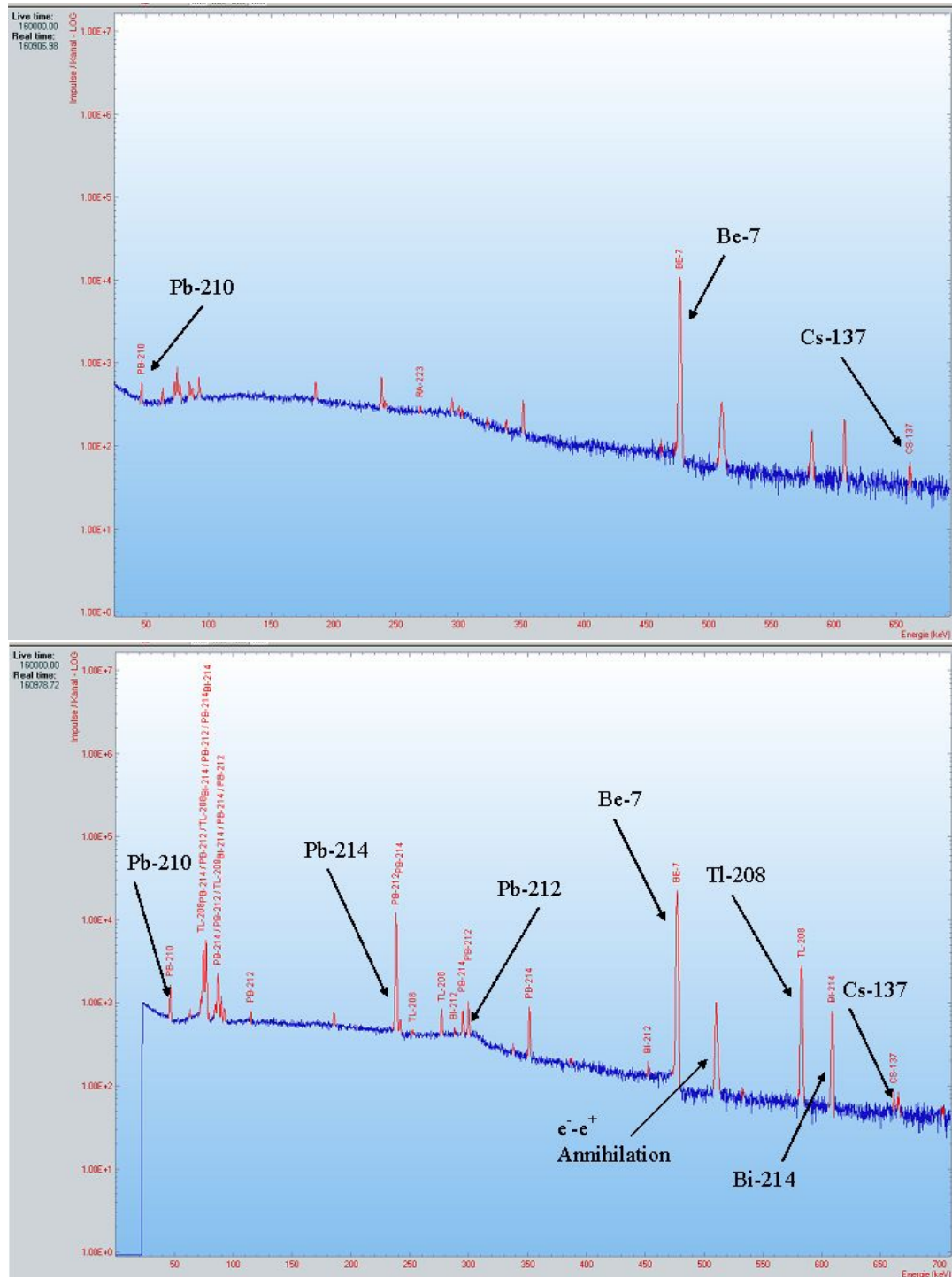


Figure 7.2: The measured spectrum of a Jungfrauoch sample on top and a Fribourg sample below. One observes that much more lines are present in the Fribourg sample. This is because we measure also the short lived daughter nuclides of Radon 222 and Radon 220 namely Bismut and Lead which are in much smaller concentration at Jungfrauoch and further have already decayed until the start of measurement. In Fribourg the filters are measured within 8 minutes after filter change and those nuclides are still on the filter.

Figure 7.3: Radioisotopes measured on filters from Fribourg. The short lived daughter nuclides of ^{222}Rn represented by ^{214}Pb have the highest activity. ^{137}Cs was undetectable most of the time. One observes the correlation of ^{214}Pb and ^{212}Pb as well as of ^7Be and ^{210}Pb .

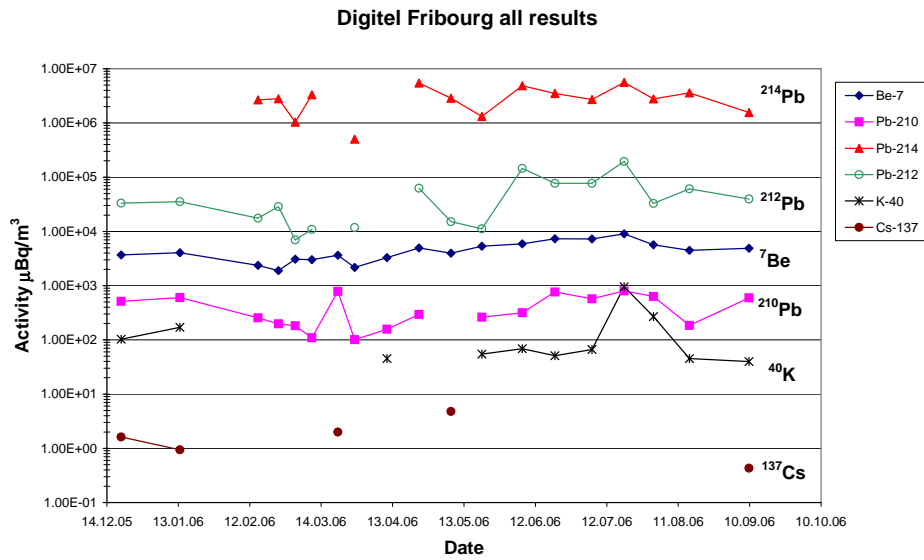


Figure 7.4: Anticorrelation of rain and ^{214}Pb activity in Fribourg

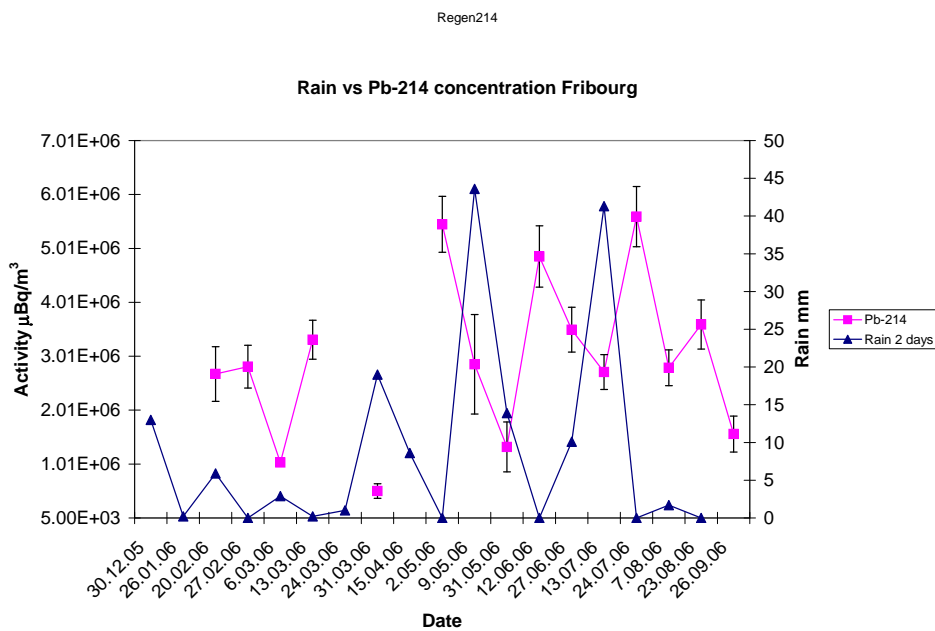


Table 7.1: Radioisotopes measured on filters from Fribourg. Activities are given in $\mu\text{Bq}/\text{m}^3$, precipitation in mm. The total uncertainty for ${}^7\text{Be}$ amounts to 6% for all the measurements. The precipitation during the sampling periods is summed and the precipitation of the last 2 days and the last day of each sampling period is given in order to see the effect on the short lived nuclides ${}^{214}\text{Pb}$ and ${}^{212}\text{Pb}$.

Start	End	Date	${}^7\text{Be}$	${}^{210}\text{Pb}$	$\frac{dA}{A}$	${}^{40}\text{K}$	$\frac{dA}{A}$	${}^{137}\text{Cs}$	$\frac{dA}{A}$
9.12.05	30.12.05	20.12.05	3.69E+03	5.13E+02	13%	1.03E+02	21%	1.62E+00	32%
30.12.05	26.01.06	13.01.06	4.05E+03	6.06E+02	11%	1.71E+02	13%	9.39E-01	49%
10.02.06	20.02.06	15.02.06	2.37E+03	2.55E+02	43%				
20.02.06	27.02.06	24.02.06	1.90E+03	1.98E+02	76%				
27.02.06	6.03.06	3.03.06	3.08E+03	1.82E+02	33%				
6.03.06	13.03.06	10.03.06	3.02E+03	1.09E+02	33%				
13.03.06	24.03.06	20.03.06	3.63E+03	7.85E+02	14%			2.00E+00	34%
24.03.06	31.03.06	28.03.06	2.17E+03	1.01E+02	44%				
31.03.06	15.04.06	10.04.06	3.29E+03	1.57E+02	48%	4.54E+01	60%		
15.04.06	2.05.06	24.04.06	4.97E+03	2.94E+02	31%				
5.05.06	9.05.06	7.05.06	3.98E+03					4.80E+00	44%
9.05.06	31.05.06	20.05.06	5.33E+03	2.62E+02	21%	5.46E+01	38%		
31.05.06	12.06.06	6.06.06	5.91E+03	3.16E+02	44%	6.89E+01	58%		
12.06.06	27.06.06	20.06.06	7.35E+03	7.67E+02	16%	5.11E+01	62%		
27.06.06	13.07.06	5.07.06	7.28E+03	5.72E+02	18%	6.66E+01	43%		
13.07.06	24.07.06	19.07.06	9.05E+03	8.00E+02	23%	9.52E+02	7%		
24.07.06	7.08.06	31.07.06	5.67E+03	6.31E+02	9%	2.70E+02	14%		
7.08.06	23.08.06	15.08.06	4.49E+03	1.72E+02	44%	4.52E+01	62%		

Start	End	Date	${}^{214}\text{Pb}$	$\frac{dA}{A}$	${}^{212}\text{Pb}$	$\frac{dA}{A}$	Rain(Σ)	2 days	1 day
9.12.05	30.12.05	20.12.05			3.34E+04	6%	22	13	13
30.12.05	26.01.06	13.01.06			3.54E+04	7%	36.3	0.2	0.2
10.02.06	20.02.06	15.02.06	2.68E+06	19%	1.76E+04	6%	33.4	5.9	0.4
20.02.06	27.02.06	24.02.06	2.81E+06	14%	2.86E+04	6%	0.6	0	0
27.02.06	6.03.06	3.03.06	1.03E+06	7%	6.97E+03	54%	43.9	2.9	1.4
6.03.06	13.03.06	10.03.06	3.31E+06	11%	1.09E+04	11%	21.1	0.2	0
13.03.06	24.03.06	20.03.06					16.6	1	0.6
24.03.06	31.03.06	28.03.06	5.05E+05	27%	1.18E+04	7%	69.3	19	0
31.03.06	15.04.06	10.04.06					151.7	8.6	8.6
15.04.06	2.05.06	24.04.06	5.45E+06	10%	6.27E+04	6%	49.3	0	0
5.05.06	9.05.06	7.05.06	2.86E+06	32%	1.52E+04	6%	48	43.6	3.3
9.05.06	31.05.06	20.05.06	1.32E+06	35%	1.12E+04	6%	116.2	13.9	1.8
31.05.06	12.06.06	6.06.06	4.85E+06	12%	1.45E+05	6%	5.1	0	0
12.06.06	27.06.06	20.06.06	3.50E+06	12%	7.70E+04	6%	68.1	10.1	10.1
27.06.06	13.07.06	5.07.06	2.71E+06	12%	7.70E+04	6%	74.2	41.3	41.3
13.07.06	24.07.06	19.07.06	5.59E+06	10%	1.96E+05	6%	42.4	0	0
24.07.06	7.08.06	31.07.06	2.79E+06	12%	3.28E+04	6%	62.4	1.7	0
7.08.06	23.08.06	15.08.06	3.59E+06	13%	6.09E+04	6%	153.3	0	0

Table 7.2: Isotopes measured at Jungfraujoch. Activities in $\mu\text{Bq}/\text{m}^3$. The relative uncertainty $\frac{dA}{A}$ for ${}^7\text{Be}$ amounts to 6%.

Start	End	Date	${}^7\text{Be}$	${}^{210}\text{Pb}$	$\frac{dA}{A}$	${}^{40}\text{K}$	$\frac{dA}{A}$	${}^{137}\text{Cs}$	$\frac{dA}{A}$
10.05.06	23.05.06	17.05.06	5.43E+03	2.25E+02	42%	1.02E+02	31%	2.37E+01	8%
23.05.06	6.06.06	30.05.06	4.46E+03	1.24E+02	66%	4.11E+01	76%	1.00E+01	12%
6.06.06	20.06.06	13.06.06	9.31E+03	5.52E+02	9%	2.88E+02	12%		
20.06.06	4.07.06	27.06.06	9.81E+03	4.78E+02	21%	5.56E+01	57%		
4.07.06	18.07.06	11.07.06	8.44E+03	3.21E+02	29%	9.12E+01	36%		
18.07.06	1.08.06	25.07.06	8.78E+03	5.46E+02	18%	6.54E+01	49%	2.64E+00	30%
1.08.06	15.08.06	8.08.06	3.99E+03	1.34E+02	16%				
15.08.06	29.08.06	22.08.06	5.88E+03	1.40E+02	55%			1.54E+00	44%
29.08.06	12.09.06	5.09.06	7.12E+03	3.95E+02	24%	8.19E+01	40%		
12.09.06	26.09.06	19.09.06	4.13E+03	3.19E+02	11%	2.76E+02	12%		
26.09.06	10.10.06	3.10.06	5.29E+03	1.70E+02	49%				

7.4.1 Results

Again, the three main elements detected are ${}^7\text{Be}$, ${}^{210}\text{Pb}$ and ${}^{40}\text{K}$. The short lived radon daughter nuclides are undetectable because of the snow and ice covering the rocks and the small part captured on the filter decays until the start of measurement. In four of nine samples ${}^{137}\text{Cs}$ was detected and had an appreciable activity of $23 \mu\text{Bq}/\text{m}^3$ on the 17th of May. This higher activity was also confirmed by the colleagues of the PTB in Braunschweig/Germany and DWD Berlin. They measured $6 \mu\text{Bq}/\text{m}^3$ [22] which is 10 times the mean concentrations measured in Braunschweig in 2006 respectively $25 \mu\text{Bq}/\text{m}^3$ in Berlin. The Polish Central Laboratory for Radiological Protection did also measure an enhanced ${}^{137}\text{Cs}$ activity concentration of $5.5 \mu\text{Bq}/\text{m}^3$ in week 18 2006 [24]. ${}^{137}\text{Cs}$ shows higher concentrations at higher altitudes than in the Swiss plateau. This high value of $23 \mu\text{Bq}/\text{m}^3$ represents the highest value measured in air in Switzerland in 2006. The activities of ${}^7\text{Be}$ and ${}^{210}\text{Pb}$ correlate and tend to a common maximum in July, decrease again in August due to precipitation.

At Jungfraujoch precipitation data are not available because most of the times the precipitation is in form of snow and the quantity cannot be measured because of the wind transporting and accumulating snow. But knowing the weather situation in the region one can tell qualitatively that precipitation washed out some activity in August. The highest values are $9.81 \text{ mBq}/\text{m}^3$ for ${}^7\text{Be}$ and $552 \mu\text{Bq}/\text{m}^3$ for ${}^{210}\text{Pb}$. ${}^{40}\text{K}$ reached its maximum of $288 \mu\text{Bq}/\text{m}^3$ in June. Our results are compared in table 7.3 to results from Tobler et al. measured in the years 2000 and 2001 [9]. The results show good agreement in ${}^{210}\text{Pb}$ data and lower activities in ${}^7\text{Be}$. Two reasons explain this: First our results represent only May-August, season in which concentrations are higher and second solar activity was on its maximum in 2000 and Beryllium production was therefore lowest, because cosmic radiation decreases when solar activity increases.

Table 7.3: Comparison of Pb-210 and Be-7 at Jungfraujoch and Fribourg. Results of the years 2000 and 2001 are to find in [9]. This year's Be-7 values are higher due to smaller solar activity than in 2000-01.

	Be-7 Jungfraujoch			Fribourg
	mBq/m³			mBq/m³
Year	2000	2001	2006	2006
			10.5.-10.10.	1.1.-26.9.
Average	5.7	5.52	6.60	4.53
Stand. Dev.	2.87	3.15	2.17	1.95
Maximum	14.7	19.6	9.81	9.05
Minimum	0.43	0.55	3.99	1.90
	Pb-210 Jungfraujoch			Fribourg
	mBq/m³			mBq/m³
Year	2000	2001	2006	2006
			10.5.-10.10.	1.1.-26.9.
Average	0.38	0.31	0.30	0.40
Stand. Dev.	0.24	0.2	0.16	0.25
Maximum	1.12	1.3	0.52	0.80
Minimum	<0.23	<0.23	0.12	0.10

7.5 Comparison Jungfraujoch-Fribourg

The trends in ^7Be and ^{210}Pb are the same at both locations. Higher concentration of ^7Be at Jungfraujoch match the higher concentration of ^{210}Pb in Fribourg. Both results are as expected, because the production of ^7Be increases with increasing altitude to reach a maximum between 17-20 km. Descending the troposphere a part of the ^7Be decays ($T_{1/2} = 53.3$ days, residence time 10-30 days). For the ^{210}Pb it is exactly the contrary ^{210}Pb is a daughter nuclide of ^{222}Rn ascending from the soil into the atmosphere. Even if ^{210}Pb can reach appreciable altitudes, it comes down by the same mechanisms as ^7Be . Its concentration at lower altitudes should be higher, because of the direct contribution of the short lived ^{214}Bi on the filter decaying into ^{210}Pb . ^{214}Bi does not reach Jungfraujoch in high concentrations.

The high ^{137}Cs concentration in May was partly detected in Fribourg and at the PTB in Braunschweig Germany where a value of $6 \mu\text{Bq/m}^3$ was measured indicating that ^{137}Cs was widespread in May. The Cesium values at Jungfraujoch are always higher than those in Fribourg. ^{40}K concentrations undergo the same variations and are slightly higher in Fribourg maybe a consequence of agriculture.

Two samples each could be measured for the long lived ^{10}Be ($T_{1/2} = 1.5 \cdot 10^6\text{y}$) content in Fribourg and at Jungfraujoch. Juerg Beer and his team from EAWAG provided the results for ^{10}Be measured at the ETH Zurich by accelerator mass spectrometry.

Figure 7.5: The ^7Be concentration is higher at Jungfrauoch whilst the ^{210}Pb activity is higher in Fribourg due to their different origin.

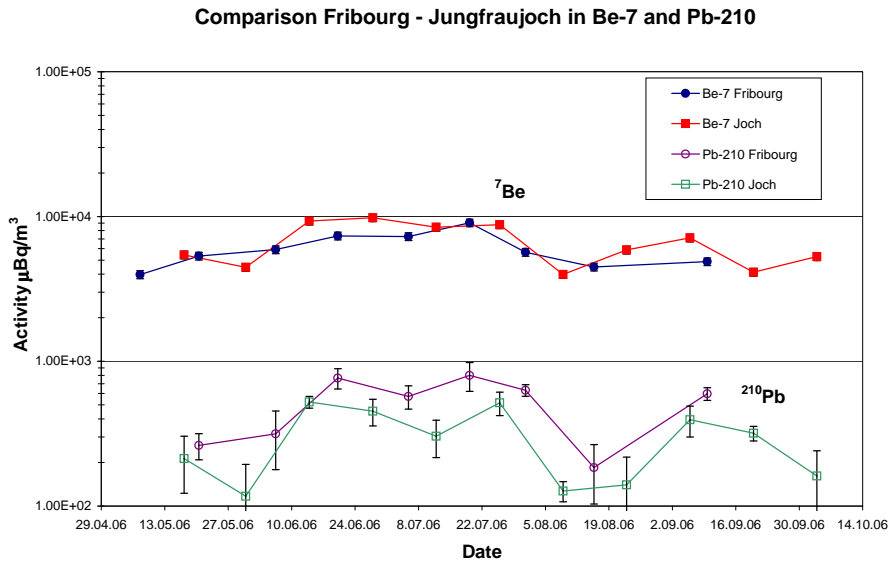


Figure 7.6: PTB, DWD and Fribourg in comparison for ^7Be . The values follow more or less the same curves. Our data peaks in July whilst german values peak already in May. Differences can partly be explained by different weather conditions.

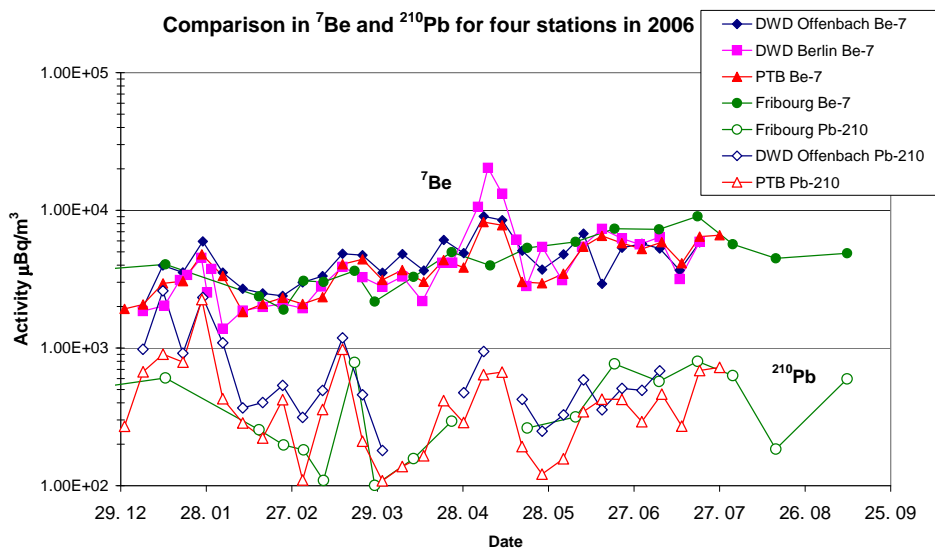


Table 7.4: $^{10}\text{Be}/^{7}\text{Be}$ ratio (R). ^{10}Be measured at ETH Zurich by accelerator mass spectrometry. Values are higher in Fribourg due to decaying ^7Be . The date corresponds to the middle of the two week sampling interval.

Date	$^{10}\text{Be}/^{7}\text{Be}$	$\frac{dR}{R}$
27.06.06	1.5	16%
25.07.06	1.5	21%
5.07.06	2.1	31%
31.07.06	2.4	26%

The results of the ratio $^{10}\text{Be}/^{7}\text{Be}$ are listed in table 7.4. The ratio of greater than 2 in Fribourg is significantly different from the one of 1.5 measured at Jungfrauoch indicating the cosmogenic origin of both Beryllium isotopes which come from the upper atmosphere and ^7Be has thus time to decay partly before reaching Fribourg whilst ^{10}Be remains constant during this sedimentation time of some days. Our values of 1.5 are inferior to values measured by Zanis [10] in the year 2000: Between 1.5 and 3 with an annual mean of 1.97 and a clear maximum in May and June. The corresponding values in June and July 2000 are approximately 2.5 and 2. This higher value could be indicative for stratospheric intrusions.

7.5.1 Comparison of the Swiss results to those of PTB and DWD

The comparison of our results to those from german institutes PTB (Physikalisch Technische Bundesanstalt Braunschweig) and DWD (Deutscher Wetterdienst Berlin and Offenbach), especially for the more or less homogeneous widespread natural ^{210}Pb and ^7Be , are shown in figure 7.6 ([22]; [23]). The german institutes provide weekly measurements, while ours are less periodically. December to April are the months in which the results follow the same curves. German values peak in May whilst ours peak in July. Weather could be a possible explanation for this difference. The remarkable high concentration of $23 \mu\text{Bq}/\text{m}^3$ ^{137}Cs at Jungfrauoch in May was also detected at PTB, where the concentration of $6 \mu\text{Bq}/\text{m}^3$ was up to 10 times higher than in other weeks.

7.6 Air radioactivity sampling with aircraft of the Swiss army in the lower stratosphere

The SUER runs a contract for six yearly flights with the Swiss Army Airforce in Payerne. A Tiger F-5E/F is equipped with two filterboxes beneath the wings. For each flight, we have two samples from the lower stratosphere. The samples are normally taken about 1 km above the tropopause. The 2005 and first 2006 results are listed in table 7.5. In 2005, both filters old and new were in use together whilst in 2006 only the new filter was used. As explained in chapter 4, the ^7Be concentration is much higher at

Table 7.5: Filters from sampling flights in the stratosphere with a Swiss army aircraft. Usually the samples are taken approximately 1 km above the tropopause (TP). l and r stand for left and right filter device, o and n for old and new filter material. The difference between the new and the old filter for the same measurement is given in the last column. The ${}^7\text{Be}$ activities A are given in $\mu\text{Bq}/\text{m}^3$. The average value amounts to $137 \text{ mBq}/\text{m}^3$. dA/A is the relative uncertainty in %.

Date	l-r; o-n	Altitude[m]	TP[m]	${}^7\text{Be}$	dA/A	Diff. n-o
25.05.05	l-o	13411	12497	1.54E+05	2%	
25.05.05	r-n	13411	12497	1.61E+05	3%	+5%
28.06.05	l-o	13320	12192	7.74E+04	3%	
28.06.05	r-n	13320	12192	8.93E+04	3%	+15%
8.07.05	l-o	9600	8534	7.97E+04	3%	
8.07.05	r-n	9600	8534	7.40E+04	3%	-7%
21.09.05	l-o	12040	11034	1.10E+05	3%	
21.09.05	r-n	12040	11034	5.32E+04	3%	-52%
26.09.05	l-o	12947	11521	2.06E+05	3%	
26.09.05	r-n	12947	11521	2.85E+05	3%	+38%
07.11.05	l-o	13106	12192	1.55E+05	3%	
07.11.05	r-n	13106	12192	4.67E+04	3%	-70%
09.05.06	l-n	10670	9753	2.28E+05	2%	-
09.05.06	r-n	10670	9753	1.73E+05	2%	-
21.06.06	l-n	11674	11765	1.53E+05	3%	-
21.06.06	r-n	11674	11765	1.45E+05	3%	-

high altitudes than at Jungfraujoch and Fribourg because of the long residence times of aerosols and the greater production rate. The difference between the left and right filter are probably due to the difference in filter quality. The average value of ${}^7\text{Be}$ amounts to $137 \text{ mBq}/\text{m}^3$ compared to 4.5 and $7.2 \text{ mBq}/\text{m}^3$ in Fribourg and at Jungfraujoch. Zanis [11] cites values at northern mid-latitudes of $18 \text{ mBq}/\text{m}^3$ at tropopause level and $155 \text{ mBq}/\text{m}^3$ in the lower stratosphere corresponding to our average value. The huge difference between the new and the old filter paper on 7th of November 2005 cannot only be due to the different manufacturer but an error in sampling may have occurred with erroneous sampling volumes. Further measurements with both filters would be necessary in order to conclude which filter is better for those types of measurements where the air flow velocity is high. The goal of such measurements would be to find a correction factor for the new filter, because the old filter was calibrated in a wind channel in Emmen and results should be accurate. The sampled air mass Q is a function of the flight velocity v and of the altitude h according to equation 7.1:

$$Q = f(v, h); \quad [Q] = [\text{kg}/\text{s}]; \quad [v] = [\text{Mach}]; \quad [h] = [\text{km}] \quad (7.1)$$

7.7 Correlation to precipitation

Scavenging by precipitation is the main process bringing the aerosols down to earth's surface. The relation of the amount of precipitation and radioactivity in air shall be determined. Our data in Fribourg are evaluated with rain and snow data from Tafers (5 km far from the sampling station) and past data from the HVS-1 station in Oberschrot (Fr) are taken together with Meteo Suisse data from the same location.

7.7.1 Oberschrot

The ^7Be and ^{210}Pb data of the HVS-1 station in Oberschrot are taken together with precipitation data in order to reproduce seasonal variations in radioactivity concentrations and correlation with precipitation. Figures 7.7 and 7.8 show that the peak concentration of both radionuclides did not appear at the same time but both occurred during the warm period of the year. One can clearly observe the anticorrelation between rain and radioactive concentrations. In 2004, both nuclides reached maximum in September. A clear and constant increase happened from January to September. In 2005, a decrease is observed in August due to heavy precipitation (flood in Switzerland 22nd-24th of August). In general both activities correlate, if the one increases the other one does increase too. In figure 7.9, weekly measurements of ^7Be are plotted versus summed precipitation in the same weeks. The anticorrelation is evident. Else one observes that rain in one week influences also the result of the following week (figure 7.9) even if it is dry. This depends on the altitude of the rainclouds and up to where the aerosols are washed out.

7.7.2 Fribourg

The precipitation data provided by Meteo Suisse were not available in 2006 until the 15th of July. Therefore the data of Tafers were taken. This station is even nearer to the physics department than the station named Fribourg placed at Grangeneuve. The results were summed in order to cover the same periods as filter samples. For the short lived radionuclides ^{214}Pb and ^{212}Pb the precipitation of the day before and the day of measurement is taken (figure 7.4). If it was raining the day before or the same day of filter change the activities are lower. This anticorrelation is evident. Else, the ^7Be concentration decreased in August when precipitation increased.

7.7.3 Fine dust concentrations

In January and February 2006, fine dust emission and concentration in air due to the inversion situation and fog were discussed extensively in newspapers and the limit of $50\mu\text{g}/\text{m}^3$ was much exceeded. In Lausanne for example a concentration of $267\mu\text{g}/\text{m}^3$ ("La Liberté" 4.2.06) was measured on February 3rd. I decided then to weigh

Figure 7.7: Rain and activity in Oberschrot 2004. The ^7Be activity increases from January til September.

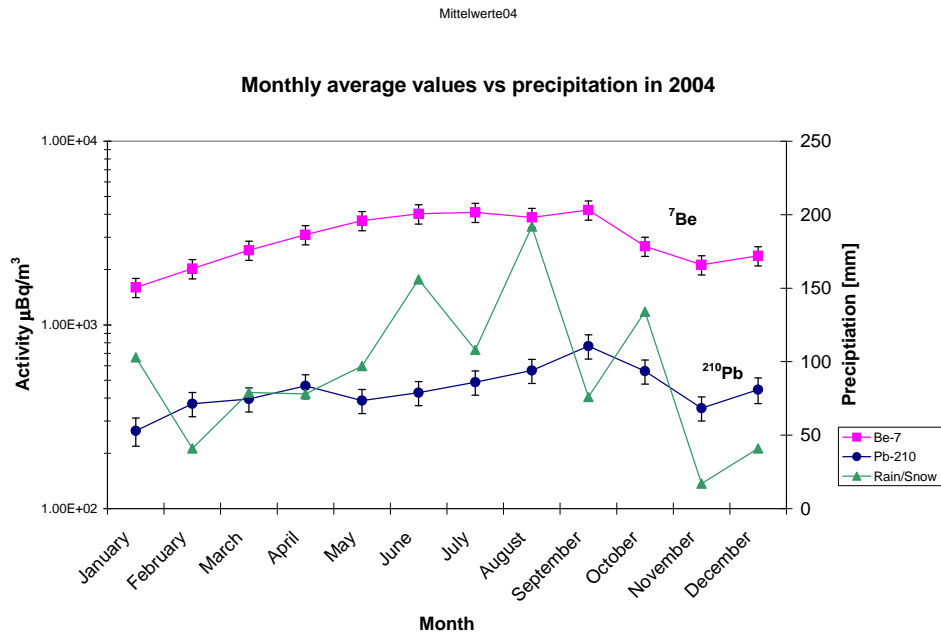


Figure 7.8: Rain and activity in Oberschrot 2005. The huge amount of rain in August led to an important decrease in the activity.

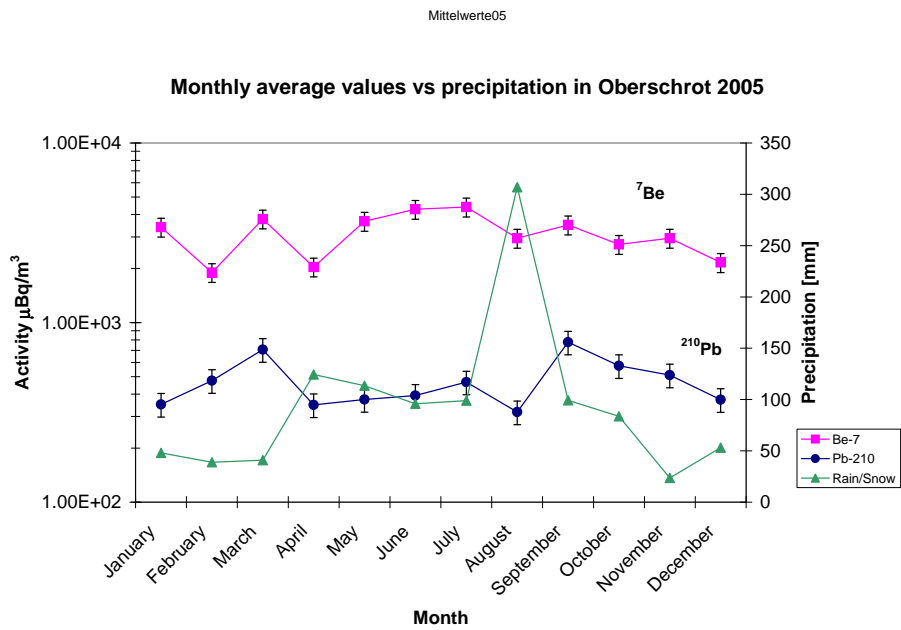


Figure 7.9: Rain vs ^7Be in spring 2004 in Oberschrot. One clearly observes opposite peaks in rain and activity. Scavenging by precipitation is the main process washing tropospheric aerosols out.

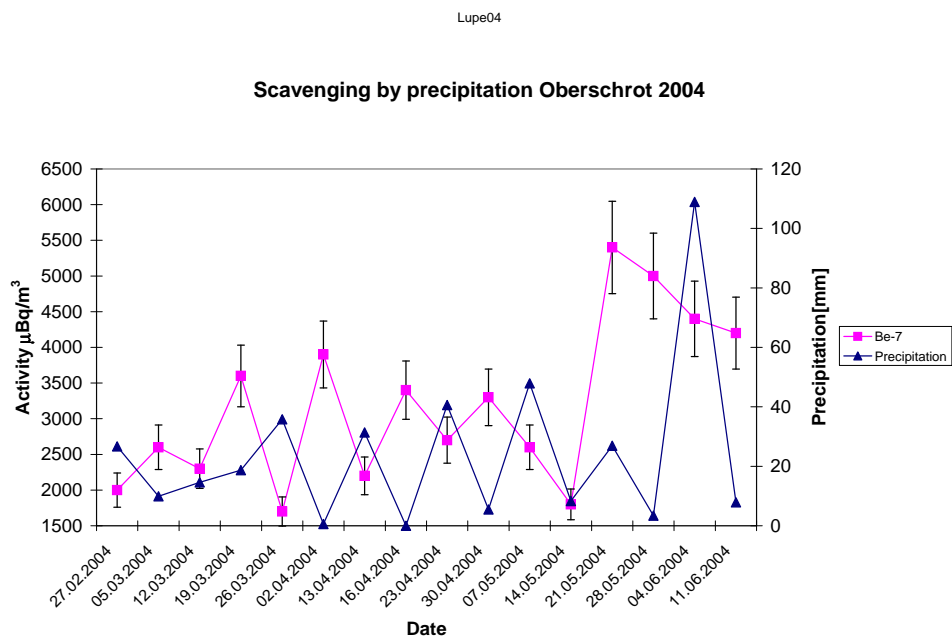


Table 7.6: Fine dust concentrations PM 10 (Particulate Matter smaller than $10\mu\text{m}$) in Fribourg summer 2006. The limit set by the Swiss law is $50\mu\text{g}/\text{m}^3$. In Switzerland concentrations are usually the highest in winter during inversion situations, when a thick fog layer prevents black carbon dust particles to move away. In February a maximum of $267\mu\text{g}/\text{m}^3$ was reached in Lausanne.

Concentration $\mu\text{g}/\text{m}^3$	Uncertainty $\mu\text{g}/\text{m}^3$	Period
23.6	0.6	8.7.-13.7.06
28.2	1.3	13.7.-15.7.06
26.5	0.7	15.7.-19.7.06
29.4	0.9	19.7.-22.7.06
21.4	0.8	22.7.-24.7.06
29.4	0.9	24.7.-26.7.06
19.6	0.6	26.7.-30.7.06
12.3	0.4	30.7.-4.8.06
9.6	0.4	4.8.-7.8.06
16.5	0.5	7.8.-11.8.06
6.7	0.4	11.8.-14.8.06
12.2	0.5	14.8.-18.8.06
11.1	0.4	18.8.-23.8.06

the sampled filters, but had to take an average for the unsampled filter mass. In the same period I obtained results between 80 and $150\mu\text{g}/\text{m}^3$ but affected of a 10% uncertainty. The higher value in Lausanne must be due do higher traffic and also the fact that Lausanne is a bigger city and has therefore more chimneys to pollute the air. Starting in July again the filters from Fribourg were weighed before and after to obtain a more precise result. The results for our filters are listed in table 7.6.

Fine dust concentrations at Jungfrauoch are much smaller ($< 5\mu\text{g}/\text{m}^3$), except for large Saharan dust events, as happened from 16th to 22nd of June ([14]). Those events could also be seen on our filters see figure 7.10. The data from Jungfrauoch are provided by Martin Steinbacher from EMPA Dübendorf [25]. This group runs a Digital HVS at Jungfrauoch and weighs the filters but these values here are obtained through a Betameter. The dust particles stick to a filter and weaken the intensity of the used ^{85}Kr β -particles. This weakening corresponds to a certain fine dust concentration (Total suspended particles). The concentrations are the lowest in winter with monthly average concentrations of $1-3\mu\text{g}/\text{m}^3$. As soon as the earth begins to warm in spring and summer, convection is increasing and dust particles are transported upwards. For this reason Jungfrauoch can no more be considered as a background station in summer. In May, the average was $3.8\mu\text{g}/\text{m}^3$. In June, there was a large Sahara dust event and a maximum value of $92\mu\text{g}/\text{m}^3$ was measured on the 20th of June. In July the average was $7.3\mu\text{g}/\text{m}^3$ and again higher due to convection.

Figure 7.10: 2 filters sampled by EMPA with a Digital DHA-80. The filter on the right shows clearly the influence of the Saharan dust event with its brown-red color. Those filters were sampled for 24 hours. Source EMPA.



7.8 Test of filtering material

The SUER runs different high volume samplers and a system for alpha and beta radioactivity called RADAIR. All those systems are based on collecting and measuring aerosols on filter material. The collection efficiency of a filter is defined as a fraction of particles collected on the filter of the particles in the air entering the filter. Collection efficiency of the aerosols depends on the filter structure, the particle size and face velocity. It is typically the lowest for particles of about $0.1\text{-}0.3\ \mu\text{m}$ [18]. Particles of this size are most easily able to follow the air flow through the porous filter. Super-micrometer particles have too much inertia to follow the curved air flow, and are deposited on the filter fibers due to impaction. Particles finer than $0.1\ \mu\text{m}$ experience substantial Brownian motion and this increases the probability to collide on filter fibers.

The different systems are equipped with different filter materials. The large ASS-500 high volume samplers use a Petryanov FPP-15-1.5 poly vinyl chloride filter, Digital uses the Ederol glass fibre filter, RADAIR Whatman glass fibre, the alert station high volume sampler in Fribourg uses a combination of celluloid and activated charcoal Staplex filters and finally a celluloid filter paper is used for the sampling at high altitudes with a Swiss army aircraft. There a new filter of the company Schleicher&Schuell is in use now since 2005, because the old one was no longer produced.

As the two Digital samplers had different software problems to solve, the engine could not be moved to Jungfrauoch until those problems were solved. So we had the opportunity to run both samplers at the same time one next to the other and test the different filter materials in comparison to the Ederol glass fibre filter 227/1/60. Collecting time was between 7-17 days and always 4 filters were sampled and measured immediately after

the last filter change. Each filter in use was tested against the Ederol filter and the obtained results are given (table 7.7) in percent relative to the Ederol filter used in the same period. The two different filters types in use were used in the two machines side by side and filter changes always happened at the same time.

During those filter tests the software of the HVS-2 has been updated twice until no more serious problems occurred.

In table 7.7 the comparison of the five different filters in use by the SUER to the corresponding Ederol glass fibre filter is given for the natural occurring radionuclides ^7Be and ^{212}Pb with uncertainties in the range of 5 to 10%. The values are given in percent respective to the activity on the Ederol filter.

The first filter in comparison was the new celluloid filter (HF new) used in aircraft sampling in use since 2005 when the samplers have been adapted to the new aircraft of the Swiss army. Its flow resistance was much smaller than that of the Ederol filter and the measurement confirmed the assumption that not all the aerosol particles were retained in the filter but passed through it. It contained only 17% and 9% of the respective activities in ^7Be and ^{212}Pb .

The old filter (HF old) of the same paper material, which is no longer produced, presents better values with 60% and 33% compared to Ederol. Its flow resistance was also clearly smaller than Ederol's but slightly higher than HF new's. It seems to be clear that this celluloid filter type is not suitable for the HVS measurement purpose. In this indirect comparison the old filter seems to be better than the new one retaining more aerosol particles.

The next filter in test was the one used in all 5 HVS-1 stations in Switzerland. The Petryanov filter FPP-15-1.5 (Pet) is made of chlorinated polyvinyl chloride and its values are in the same range as Ederol's. 103% for ^7Be and 84% for ^{212}Pb . Considering the uncertainties and the fact that different detectors are used the performance seems to be almost the same. Its efficiency is tabulated to be $\geq 95.6\%$ at $0.2 \mu\text{m}$. The same results are obtained with the other type of Petryanov used by the Radioactivity Section in Bulgaria (Pet Bul).

The fourth filter used in the alert high volume station in Fribourg was of different size. Its diameter is 10.16 cm and a cardboard form had to be made in order to fix the filter on the filter holder and to ensure that the air flows through the filter. The Staplex TFA # 2133 filter provided almost the same results as the Petryanov filters but also slightly smaller activities were obtained suggesting that not all the aerosols remain clinged. Its tabulated efficiency at $0.5 \mu\text{m}$ is 95%.

Finally a second glass fibre filter was tested. The same one is in use in the RADAIR stations where it is rolled. Here, we used the same geometry of 150 mm round Whatman filters. The results show higher values for every nuclide: 104% for ^7Be and 115% for ^{212}Pb .

Table 7.7: Filters in relation to the Ederol glass fiber filter

	Ederol	HF new	HF old	Pet	Pet Bul	Staplex	Whatman
Be-7	100%	17%	60%	103%	94%	54%	104%
Pb-212	100%	9%	33%	84%		66%	115%

The disappointing result of the new celluloid filter HF new gave reason for another test with two filters each time on the same filter holder making two layers. For the measurement 4 lower and 4 upper filters were taken together. The results are listed in table 7.8. The first filter is referenced as 100%. Still 47% of ^7Be was measured on the second filter but only 6% of ^{212}Pb showing that a huge part of the aerosols go through the first filter.

The same procedure was made for the Ederol filter because the comparison to the Whatman showed that even the Ederol filter does not retain 100% of the aerosol particles. But the results are different (table 7.8): Approximately 1% of the ^7Be activity was on the second filter and 3% of the short lived ^{212}Pb . The glass fibre filter is therefore very well suited for our measurements.

The two test with the HF new filter clearly show a certain weakness versus the glass fibre filters but also versus the old HF filter. The two filters have already been used together in the 2005 aircraft campaign and the astonishing result is that in 3 of 6 flights the ^7Be values were slightly higher than those obtained with the old filter, see table 7.5. One filter was in the box below the right wing and the other below the left. But two of three times the activity was much smaller by a factor of almost 4 once! Further tests would be necessary to conclude which filter is less performing. But a lot of clues are given that the new one has some weakness. The goal would be to find an experimental correction factor in order to adjust the values obtained with the new filter, because the old filter was calibrated in a wind channel and the air volume calculates itself according to equation 7.1.

One can conclude that these tests provided good values for the glass fibre filters Ederol and Whatman as well as for the Petryanov filters. The worse result of the Staplex filter is maybe due to the setup in the filter holder, where a cardboard had to be put around the filter because of its different dimensions. It is possible, that air flowed between the filter and the cardboard or even small parts directly through the cardboard. This Staplex filter is used in the alert high volume station in Fribourg and its results are always in the same range as those from Oberschrot, where a HVS-1 is run with Petryanov filters, indicating no weakness. Those tests were accomplished only once and the results should thus be handled with care.

Table 7.8: Two filters were superposed in the same filter holder and measured separately. The activity on the upper filter takes the 100% value.

	Ederol 1st	Ederol 2nd	HF new 1st	HF new 2nd
Be-7	100%	1%	100%	47%
Pb-212	100%	3%	100%	1%

7.9 Anticorrelation of Beryllium and solar activity

Solar variations are fluctuations in the amount of energy emitted by the Sun. Small variations have been measured from satellites during recent decades. The amount of solar radiation received at the outer surface of Earth's atmosphere was once assumed to not change much from an average value of 1366 W/m^2 . The variations in total solar output are so slight (as a percentage of total output) that they remained at or below the threshold of detectability until the satellite era, although the small fraction in ultra-violet wavelengths varies by a few percent. Total solar output is now measured to vary by approximately 0.1% [13] or about 1.3 W/m^2 peak-to-trough of the 11 year sunspot cycle. Sunspots are relatively dark areas on the surface of the Sun and are thus cooler than its average surface. The number of sunspots correlates with the intensity of solar radiation. The higher the sunspot number the higher the radiation because the areas surrounding sunspots are brighter than the average and the overall effect is that more sunspots means a brighter sun. An increase in solar activity is accompanied by an increase in the solar wind, which is an outflow of ionized particles, mostly protons and electrons, from the sun. The Earth's magnetic field, the solar wind and solar magnetic field deflect galactic cosmic rays (GCR). A decrease in solar activity increases the GCR penetration of the troposphere and stratosphere. GCR particles are the primary source of ionization in the troposphere above 1 km and as explained in chapter 4 the source of ^7Be and ^{10}Be radionuclides. The production of those radionuclides depends thus on the 11 year cycle of the sun. As the intensity of galactic cosmic rays decreases when the sunspot number increases the production of Beryllium decreases too. This variation comes out on our collected beryllium measurements on figure 7.11 since the year 1991. Weekly data are averaged to quarter year values. The concentration is high in 1996-97 and is at its lowest in 1999-2002. Sunspot maximum therefore occurred in the years 1990-92 and 2000-2002 with a minimum in 1997 according to figure 7.12. Moreover one observes a clear seasonal variation in surface ^7Be concentrations, except for the years 1993, 1998 and 2000 the concentration increases in the first three quarters of the year and decreases again in winter. The average of those data collected during 16 years shows that concentration is lowest in the months January to March with $2800 \mu\text{Bq/m}^3$ and highest in the period July to September with $3800 \mu\text{Bq/m}^3$. The mean value for April to June is $3300 \mu\text{Bq/m}^3$ whereas for October to December it is $2500 \mu\text{Bq/m}^3$. Those values confirm the the fact of an increased mixing of the troposphere in the warm period of the year as explained in section 4.1.2.

Figure 7.11: Collected ^7Be data from Fribourg and Oberschrot with a clear minimum in 1999-2002 when solar activity was high. The seasonal variation of ^7Be is evident.

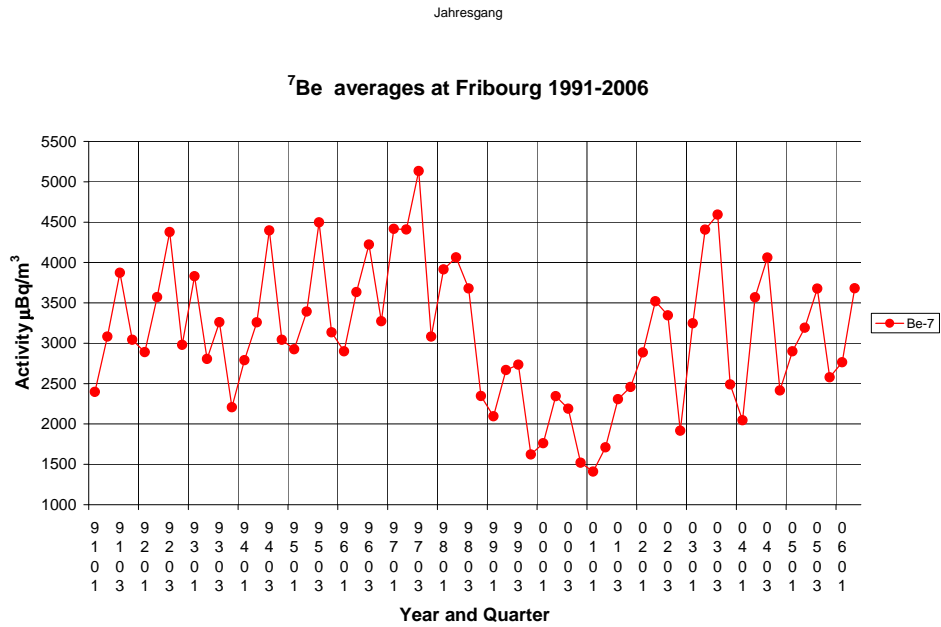
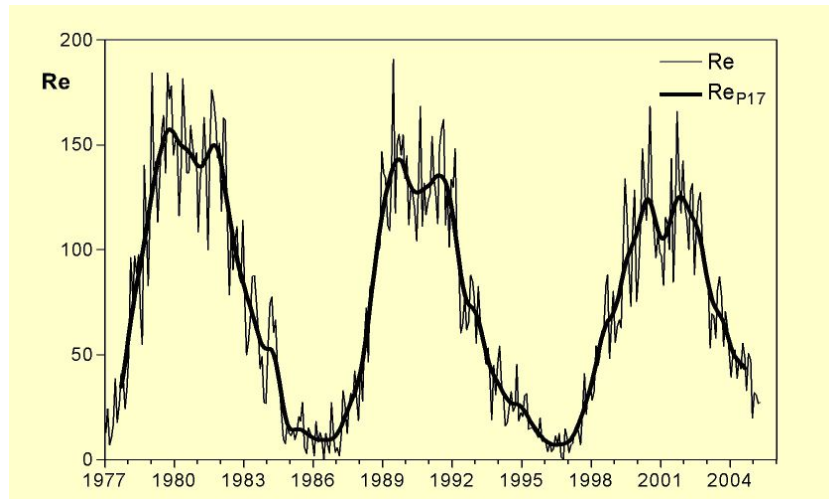


Figure 7.12: Sunspot number representing the 11 year cycle of the sun. The maximum between 2000-2002 results as a minimum in figure 7.11.



8 Conclusions

The research of this Master Thesis took place during 9 months. Because of the limited observation period it was not possible to identify seasonal variations of ^7Be and ^{210}Pb . However other measurements (Oberschrot, Zanis [11], Tobler [9]) provide these informations: They show higher concentrations in summer and lower in winter. The comparison of our data with PTB and DWD shows the homogeneous distribution of ^{210}Pb and ^7Be . ^7Be tends to be higher in Germany, as its production increases with increasing latitude. The most important part of natural radioactivity is the terrestrial component, notably the daughter nuclides of ^{222}Rn in the uranium series and those of ^{220}Rn in the thorium series. ^{137}Cs was the only artificial gamma emitter detectable at Fribourg and Jungfrauoch, but most of the time its activity was below the detection limit.

After some software problems have been solved at the beginning of this Master Thesis the Digitel samplers worked completely satisfactory. Even with a much smaller air flow volume compared to the first generation HVS-1 stations the detection limits of the nuclides are of some tens of $\mu\text{Bq}/\text{m}^3$ (see table 8.1). The sampler is controlled remotely. Due to its filter holder reservoir of 15 filters it runs independently for several weeks. The sampled volume shows only a small uncertainty of measurement.

8.1 Digitel combined with ORTEC Detective

The aim of the SUER is to improve the radioactivity monitoring network in Switzerland. To date, there are 11 RADAIR stations providing only gross beta activity every 30 minutes (Detection Limit $\sim 0.5 \text{ Bq}/\text{m}^3$) and the 5 HVS-1 systems providing individual radionuclide data every week (Detection Limit $\sim 0.3 \mu\text{Bq}/\text{m}^3$). The final goal of a Digitel sampler combined with an on-line gamma-spectroscopy is to obtain results with high sensitivity within several hours through Internet. The SUER runs a portable electric cooled gamma-ray spectrometer called "Detective" manufactured by Ortec. The idea is to modify the Digitel sampler and to combine it with a Detective placed in front of the filter. For the evaluation of the spectrum the data should be exported to a PC via FTP. One measurement was made with a 4-day-sampled filter, which was placed directly in front of the entrance window of the detector, to obtain detection limits for the different isotopes. Table 8.1 illustrates the result of this combination. In order to combine the Detective with the Digitel sampler, the construction would have to be adapted. The steering of both detector and HVS-2 should be made via Internet. Further

Figure 8.1: Digitel with the portable germanium gamma ray spectrometer "Detective" on it. The round metal cap is the entrance window of the germanium crystal and the ^{137}Cs calibration source is situated just below on the docking station. A combination of both instruments would need important modifications of the Digitel sampler.



a lead shielding should be provided to the Detective to reduce background and cosmic radiation. These arrangements would require important modifications of the sampler. Moreover the Detective must be modified; a solution has to be found especially for the on-line energy calibration. The first aim of this Master Thesis was to study the feasibility of such a combination, in order to suggest it to the manufacturer of the Digitel sampler.

8.1.1 Advantages of Digitel

The small size of the Digitel DHA-80 compared to the first generation HVS systems, and the low noise are important advantages. The Digitel can be run almost everywhere and moved quickly to another place if necessary. Also the preprogrammed times of filter changes and the constant flowrate during the whole sampling period are benefiting. Moreover the remote steering provides direct filter changes and modifications in settings during work time, such as pressure and temperature data etc. The combination of Digitel and Detective would be a great improvement of the radioactivity control network especially when fast acting would be necessary. This for example after nuclear accidents or nuclear weapon tests.

As mentioned above, the implementation of this new system would require modifications of both devices. The Detective must be remotely controllable and the implemented ^{137}Cs

calibration source must be moved out of the shielding during measurement. We suggest to use a ^{40}K source on a filter for the energy calibration. ^{40}K emits one single gamma-ray at an energy of 1460 keV. For the measurement this calibration filter should be removed and replaced by the sampled filter ready for measuring.

8.2 Detection Limits

Three systems for radioactivity monitoring have been compared for the detection limits and the time interval until the results are available. In table 8.1 the values are given in $\mu\text{Bq}/\text{m}^3$ for four different radionuclides. It is to be said that the HVS-1 systems collect up to 10 times the volume of Digitel; its detection limit is therefore lower. For two reasons the detection limit for the combination Digitel-Detective is higher: firstly only one filter has been measured, whereas in the laboratory 4 filters are measured with 4 times the volume. Secondly the germanium crystal of the Detective is smaller and thus less efficient than the Ge-crystals used in the laboratory. Doubling the sampled volume improves the detection limits to about a factor of $\sqrt{2}$. The detection limit for the HVS-1 sampling stations is about 10 times lower and the same factor lies between measuring Digitel filters in the laboratory or directly on the Detective. The detection limit for ^{137}Cs in the combination of Digitel and Detective is $30 \mu\text{Bq}/\text{m}^3$. It is, therefore, sensible enough to detect important nuclear events such as radioactive clouds as released after the Chernobyl accident in April 1986 which was in the order of $1 \text{ Bq}/\text{m}^3$. The combination of Digitel and Detective would thus be an ideal addition to the radioactivity monitoring network in Switzerland.

8.3 The GAW Program of the WMO

The GAW (Global Atmosphere Watch) Program [27] has been established by the WMO (World Meteorological Organisation) to provide measurements, scientific assessments, and other information on changes in the global chemical composition and related physical characteristics of the atmosphere. Concerning aerosols, the objective of the GAW program is to determine the spatio-temporal distribution of aerosol properties related to climate forcing and air quality up to multi-decadal time scales. Presently, GAW consists of 20 Global stations, which cover different types of aerosols: Clean and polluted continental, marine, arctic, dust, biomass burning, and free troposphere. Most of these sites are located in pristine areas. Therefore, the Scientific Advisory Group (SAG) for Aerosols and Aerosol Optical Depth recently made additional recommendations that would provide better coverage of the polluted continental aerosol type. In addition, there are about 300 Regional stations where measurements are conducted closer to the source areas. In this way, Global stations may then serve as standards for Regional stations. Priorities have been set for measurements at the Global and Regional stations. Regional stations will be expected to measure optical depth, mass concentration

Table 8.1: Description, detection limits and reaction time intervals (i.e. the time until the results are available) of the different air radioactivity monitoring systems in use in Switzerland. RADAIR providing half an hour data about α - and β -activity. HVS-1 with an air flow rate of up to 600 m³/h measuring in the laboratory by gamma spectroscopy. And the new HVS-2 Digitel measuring in the laboratory and with ORTEC Detective as a project.

Monitoring Systems	#	m ³ /h	Method	Detection Limits [$\mu\text{Bq}/\text{m}^3$]	Sampling time	Reaction time	Data Transmission
RADAIR	11	16	gross α & β calculated net artificial β -activity	$5 \cdot 10^5$ for artificial β -activity	30 min	30 min	on-line
HVS 1 st Generation ASS-500	5	600	Laboratory γ -spectroscopy	¹³⁷ Cs: \approx 0.3 ²¹⁰ Pb: \approx 10 ⁴⁰ K: \approx 10 ⁷ Be: \approx 3	1 day to 1 week	10 days	No
DIGITEL	2	< 60	Laboratory γ -spectroscopy	¹³⁷ Cs: \approx 2 ²¹⁰ Pb: \approx 130 ⁴⁰ K: \approx 50 ⁷ Be: \approx 20	1 week	10 days	No
DIGITEL plus DETECTIVE (Project)	–	< 60	on-line γ -spectroscopy	¹³⁷ Cs: \approx 30 ²¹⁰ Pb: \approx 240 ⁴⁰ K: \approx 600 ⁷ Be: \approx 100	1h to 1 day	1 day	on-line

in two size fractions, major chemical components in two size fractions, and the scattering coefficient. At Global stations, a larger number of measurements are envisaged, with optical depth, mass concentration in two size fractions, major chemical components in two size fractions, the scattering and hemispheric backscattering coefficient at various wavelengths, the absorption coefficient, aerosol number concentration, cloud condensation nuclei (CCN) at 0.5% supersaturation, as well as diffuse, global and direct solar radiation, and additional parameters to be measured intermittently. Data are managed by the World Data Center for Aerosols in Ispra (Italy), and it is planned to establish a World Calibration Center to ensure global data comparability. With the global coverage of the sites and the large number of aerosol parameters measured, the GAW aerosol program is believed to be an excellent candidate for ground truthing of satellite data.

8.3.1 The Central European Baseline Station

The European GAW Baseline station comprises the Zugspitze/Hohenpeissenberg (2962 m, Germany), the Jungfrauoch (3454 m, Switzerland) and Sonnblick (3106 m, Austria) high-alpine stations (Figure 8.2). The National Weather Institutes of all three countries have agreed to combine measurements under the DACH (Germany, Austria, Switzerland) agreement. In order to obtain as extensive a database as possible, each station will focus on a particular physical/chemical aspect of climatically important aerosol parameters.

Figure 8.2: The Central European Baseline Stations contributing to GAW Program.

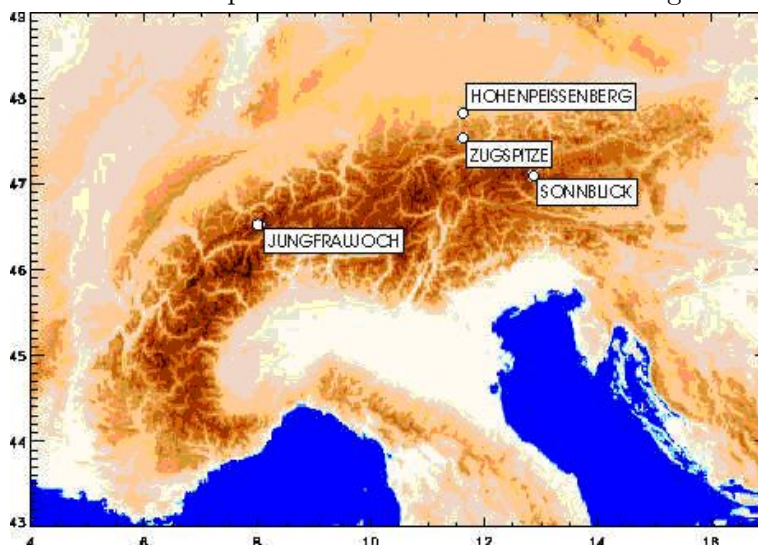


Figure 8.3: Global Atmosphere Watch Program



8.3.2 Contribution of the Radioactivity Section (SUER)

Beside all kind of weather and aerosol data the GAW Program contains also measurements of ambient radioactivity and our goal is to participate in this program in the near future. Thus we use the Digital DHA-80 and measurements are made in the laboratory with high purity germanium spectrometers. At the moment our data cover always two weeks of sampling. This sampling period can of course be adapted but should not be shorter than 1 week if the detection of ^{210}Pb and ^{40}K is requested because detection limits for both natural radionuclides would in most of the cases not be reached after only 1 week of sampling.

Bibliography

- [1] K. Krane, Modern Physics, Second Edition (1996)
- [2] J. Hemmingway: Practical Gamma-Ray Spectrometry, John Wiley&Sons (1995)
- [3] W. Stolz, Radioaktivität, 2. Auflage, Teubner (1990)
- [4] C.E Jordan, J.E. Dibb: $^{10}\text{Be}/^7\text{Be}$ tracer of atmospheric transport and stratosphere-troposphere exchange, Journal of Geophysical Research, Vol 108, NO. D8, 4234, 2003
- [5] J.E. Dibb et al. : Estimation of stratospheric input to the Arctic troposphere: ^7Be and ^{10}Be in aerosols at Alert, Canada, Journal of Geophysical Research, Vol. 99, NO. D6, 12855-12864, June 20, 1994
- [6] H.W. Feely: Factors that cause seasonal variations in Be-7 concentrations in surface air, Journal of Environmental Radioactivity, 9, 223-249, 1989
- [7] M. Yoshimori et al. : Be-7 nuclei produced by galactic cosmic rays and solar energetic particles in the earth's atmosphere, Adv. Space Res. Vol. 32, No. 12, pp. 2691-2696, 2003
- [8] M. Yoshimori: Production and behaviour of beryllium 7 radionuclide in the upper atmosphere, Adv. in Space Research, Vol. 36, 922-926, 2005
- [9] Tobler et al. : Messung von atmosphärischem ^7Be , ^{10}Be und ^{210}Pb an der hochalpinen Station Jungfraujoch, Bundesamt für Gesundheit, Abteilung Strahlenschutz, Jahresbericht Umweltradioaktivität und Strahlendosen in der Schweiz, B. 4.5.1-4.5.5 (2001)
- [10] P. Zanis et al. : An estimate of the impact of stratosphere-to-troposphere transport (STT) on the lower free tropospheric ozone over the Alps using ^{10}Be and ^7Be measurements, J.of Geophysical Research, Vol. 108, NO. D12, 8520, 2003
- [11] P. Zanis et al. : Factors controlling beryllium-7 at Jungfraujoch Switzerland, Tellus, 51B, 789-805, 1999
- [12] Prof. Dr. rer. nat. H. Bonka: Lecture "Radioökologie" WS 98/99, RWTH Aachen
- [13] www.wikipedia.org, The Free Encyclopedia
- [14] Martine Collaud Coen: Variability and long-term trends of aerosol parameters at the Jungfraujoch, Poster at the international conference for the 75th anniversary of the high altitude research station Jungfraujoch, September 2006
- [15] Christoph Wilhelm: Kalibrierung eines Gamma-Spektrometers, Forschungszentrum Karlsruhe, Kursunterlagen Februar 1998

-
- [16] Dirk Arnold: Selbstabsorptions- und Koinzidenzsumimationskorrekturen in der Gammaskpektrometrie, PTB, S0542, Kursunterlagen Februar 2002
 - [17] Nagai, H et al. : Production rates of ^7Be and ^{10}Be in the atmosphere, Nucl. Instr. Methods Phys. Res. B, 172, 781-796, 2000
 - [18] Valmari T. et al. : Aerosol sampling methods for wide area environmental sampling (WAES), STUK-YTO-TR 183, June 2002
 - [19] C. Murith et al.: KSR, internal report, 7.3.2005
 - [20] Dirk Arnold PTB: Arbeiten mit Korrekturmodulen, Forschungszentrum Karlsruhe, Kursunterlagen April 2005, S1030
 - [21] 29. Bericht der Eidgenössischen Kommission zur Überwachung der Radioaktivität für die Jahre 1985-1986
 - [22] Dr. Herbert Wershofen, PTB Braunschweig, personal communication
 - [23] Dr. Thomas Steinkopff, DWD, Langen bei Frankfurt, personal communication
 - [24] K. Isajenko, I. Kwiatkowska: Central Laboratory for Radiological Protection, Warsaw, Poland, personal communication
 - [25] Martin Steinbacher, EMPA Dübendorf, personal communication
 - [26] <http://library.thinkquest.org>
 - [27] <http://gaw.web.psi.ch>

Acknowledgements:

I would like to thank everybody who helped me during this work especially the following persons:

- My parents giving me the possibility to study what I wanted namely Physics.
- Prof. Dr. Hansruedi Völkle who welcomed me in his team and suggested me this work. He helped me whenever I had questions about physics and moreover gave me helpful advice about my future work.
- Mathieu and Matthias my colleagues working in the same beautiful office on the roof who helped me especially for computer questions.
- Alex who first forced me to write this thesis with \LaTeX . As soon as he had all the software installed on my computer there was no way out. But now I am glad that I gave way to his pressure.
- Sybille who introduced me to the program GESPECOR.
- Aline and Mathieu improving my English.
- "Wetterfrosch" Dr. Mario Slongo providing me the rain data from Tafers.
- The house keepers at Jungfrauoch sending me the sampled filters.
- My old schoolmate Simon Gasser who provided me the articles I wanted out of the ETH Zurich library.
- My girlfriend Noémie who supported me during this work and lives just next to the University, providing me thus a perfect work location.